# DEVELOPMENT OF NOVEL METHOD FOR RAPID AND ACCURATE DETECTION OF VIRAL INFECTION

**KARLA CRISTINE CALLANO DOYSABAS**

**LABORATORY OF ANIMAL MORPHOLOGY**

**DEPARTMENT OF ANIMAL SCIENCE**

**GRADUATE SCHOOL OF BIOAGRICULTURAL SCIENCES**

**NAGOYA UNIVERSITY**

**A DISSERTATION SUBMITTED IN PARTIAL FULFILLMENT FOR THE DEGREE OF**

**DOCTOR OF BIOAGRICULTURAL SCIENCE**

**MARCH 2020**

**ABSTRACT**

Adenosine 5'-triphosphate (ATP), the major energy currency of the cell, is involved in many cellular processes including the viral life cycle and can be used as an indicator of early signs of cytopathic effect (CPE). In this study, we demonstrated that CPE can be analyzed using a FRET-based ATP probe named ATeam. An ATeam probe was ligated into the pMXs-IRES-Puro to generate pMXs-ATeam-IRES-puro, which was transfected to BHK-21 cells to produce BHK-ATeam cells. The BHK-ATeam cells were infected with selected viruses and subsequently fixed with 4% PFA to inactivate the virus. The fixed cells were then examined under confocal microscope, wherein images from both Venus and cyan fluorescent protein (CFP) channels were obtained. After acquiring the intensity values from the two channels, Venus/CFP ratios were measured manually or automatically using the developed ImageJ and Python program set. Results revealed that as early as 3 h, virally infected cells showed a significantly different Venus/CFP ratio compared to the mock-infected cells. The ATeam technology is therefore useful in determining early signs of ATP-based CPE as early as 3 h without morphology-based CPE by light microscopy and enables high throughput determination of the presence of microorganisms in neglected samples stored in laboratories.

Keywords: ATeam probe, BHK-ATeam cells, FRET, cytopathic effect, viral infection

Abbreviations: ATeam, ATP indicator based on Epsilon subunit for Analytical Measurements; ATF6, activating transcription factor 6; ATP, Adenosine 5'-triphosphate; BHK-21, baby hamster kidney; BiP, binding protein; BC, boomerang catcher; BCV, Bovine Coronavirus; BEV, Bovine Enterovirus; BPIV3, Bovine Parainfluenza virus-3; BVDV, Bovine Viral Diarrhea Virus; CFP, cyan fluorescent protein; CPE, cytopathic effect; DMEM, Dulbecco's modified Eagle's medium; EMCV, Encephalomyocarditis virus; ER, endoplasmic reticulum; IRE1, ER transmembrane protein kinase/endoribonuclease; FBS, fetal bovine serum; FRET, Forster resonance energy transfer; HCV, Hepatitis C virus; HCMV, Human cytomegalovirus; IBR, Infectious Bovine Rhinotracheitis Virus; JEV, Japanese encephalitis virus; PERK, PKR-like ER kinase; Plat-E, Platinum-E; PTV, Porcine Teschovirus-ka2; RdRp, RNA-dependent RNA polymerase; ROS, reactive oxygen species; TCA, tricarboxylic acid cycle; YFP, yellow fluorescent protein

## TABLE OF CONTENTS

# General Introduction

The birth of virology is attributed to the works of Ivanovsky and Beijerinck. Dmitry Ivanovsky used the Chamberland filters and showed that leaf extracts from tobacco plants remain infectious after filtration suggesting that it can be caused by a toxin or very small bacteria. This was later known as tobacco mosaic virus. In 1898, Martinus Beijerinck concluded that the filtrate has a new form of infectious agent that can only multiply in dividing cells and he called it contagium vivum fluidum, later re-introduced as virus. In the same year, Friedrich Loeffler and Paul Frosch use the Chamberland filters to a disease in cattle and discovered the cause of foot and mouth disease. The use of the filtration criteria has revealed the association of many acute animal diseases with what are to be called viral infections such as African horse sickness, fowl plague, equine infectious anemia, classical swine fever, and etc. (Enquist and Racaniello, 2013; MacLachlan and Dubovi, 2011). Virus have been grown in solid animal tissues such as minced hen's kidney (Maitland, 1928) and embryonated eggs (Woodruff and Goodpasture, 1931). The study of viruses has further progressed until Enders and colleagues successfully cultured poliomyelitis virus single cell culture, the human embryonic cells (Enders et al., 1949). The cytopathic effect (CPE) under light microscopy as evidence of viral presence has been described and became a worldwide gold standard in viral isolation and identification (Hematian et al., 2016; Robbins et al., 1950). Since then, decades past, few improvement in the CPE methodology have been developed.

The CPE is a distinct observable morphological change in cells, easily observed through light microscopy, due to viral infection (Robbins et al., 1950). It is considered to be the result of host-defensive and anti-defensive actions that lead to non-programmed necrosis or programmed apoptosis (Itakura et al., 2019). Some

viruses cause other types of CPE. The human Immunodeficiency virus (HIV) causes syncytium formation as a result of the fusion of cells expressing surface HIV-1 envelope glycoproteins with CD4-positive cells (Kowalski et al., 1991), the bovine herpesvirus-1 causes focal degeneration along with micro plaque formation in the early phase of infection which progresses to clumping of cells in MDBK cells (Bashir et al., 2015), alpha herpesviruses can cause rounded cells with or without syncytia, while reovirus and canine distemper virus can cause inclusion bodies in Vero cells (MacLachlan and Dubovi, 2011).

Depending on the virus type, many viruses show CPE after 5-10 days of incubation except for herpes simplex virus (HSV) that produces CPE after 24 h and cytomegalovirus (CMV) that produces CPE after 10 to 30 days of incubation, while some viruses including bovine viral diarrhea (BVDV), do not show CPE (Rajput et al., 2017; Hematian et al., 2016; Leland and Ginocchio, 2007). Although hemadsorption test is another approach for detecting viruses that produce CPE slowly or not at all in cell culture; it is useful only for influenza virus, parainfluenza virus, and mumps virus (Leland and Ginocchio, 2007). Thus, a more rapid and accurate way of detecting CPE, such as the use of biomarker, as an alternative to conventional morphology-based CPE is necessary in viral isolation.

Virus, being an obligate parasite, directs cell machinery and utilizes cell resources to produce more progeny. It affects the gene expression, physiological parameters, and cellular activities of the infected cells (Albrecht et al., 1996). Thus, intracellular molecules are potential biomarker for viral infection. ATP, the major energy currency of the cell, is involved in many cellular processes including viral life cycle (Mahmoudabadi et al., 2017; Ando et al., 2012). Many viruses can upregulate

aerobic glycolytic pathways to increase ATP and the generation of metabolites for various viral processes (Chuang et al., 2017; Findlay and Ulaeto, 2015; Fontaine et al., 2015; Diamond et al., 2010). ATP is required in the replication process of vaccinia virus, for DNA assembly and capsid maturation of herpes simplex virus, for capsid assembly and release of type D retrovirus, for capsid assembly of human immunodeficiency virus, and for budding and RNA synthesis of influenza virus (Maruyama et al., 2018; Chang et al., 2009; Hui and Nayak, 2001).

It was reported that ATP promotes viral replication and is positively correlated with viral productivity (Chi et al., 2018; Chuang et al., 2017; Burgener et al., 2006). It has been shown that an infection by vaccinia virus results in an increase in ATP production by the cells due to upregulation of mitochondrial genes for proteins that are part of the electron transport chain (ETC) that generates ATP, *ND4* and *CO II* (Chang et al., 2009). Human cytomegalovirus (HCMV) upregulates glycolysis and interferes with the tricarboxylic acid cycle (TCA) to produce more NADH and ATP for virus propagation (Munger et al., 2006). ATP is also increased in viable cells after infection with baculovirus (Olejnik et al., 2004) and avian reovirus (Chi et al., 2018). In contrast, previous studies have shown that intracellular ATP is significantly decreased after viral infection (Burgener et al., 2006). This is also true in the case of Hepatitis C virus (HCV) wherein it was observed that cells involved in HCV RNA replication actively consumed ATP, thereby decreasing cytoplasmic ATP levels (Ando et al., 2012). Cellular ATP levels are also decreased after infection with influenza virus due to the massive consumption of ATP by the virus (Maruyama et al., 2018; Ritter et al., 2010). Dengue virus also promoted changes in mitochondrial bioenergetics leading to a 20%

decrease in ATP content of virally infected cells (El-Bacha et al., 2007). Thus, ATP level is another biomarker for virus infection alternative to the morphology-based CPE.

Recently, a genetically encoded Forster resonance energy transfer (FRET)-based ATP probe was developed. In this system, the ε subunit of $F_oF_1$-ATP synthase is sandwiched between cyan fluorescent protein (CFP) and yellow fluorescent protein (YFP) (Nakano et al., 2011; Imamura et al., 2009). This probe has been used by many studies for real-time visualization and measurement of intracellular ATP (Chi et al., 2018; Depaoli et al., 2018; Lerchundi et al., 2018; Chuang et al., 2017; Conley et al., 2017; Toloe et al., 2014; Tsuyama et al., 2013). However, the application of ATeam for identification of early signs of CPE has not yet been developed.

In Chapter 1, the author investigated the early signs of CPE in virally infected cells through ATP measurement using ATeam technology (ATP-based CPE).

In Chapter 2, the author developed a software program that is more rapid, more convenient, more objective, and automatically select and calculate FRET in cells.

# Chapter 1:

# ATeam Technology is a rapid and accurate way to determine ATP-based CPE by viral infection

## Introduction

Recently, bats have been discovered as natural reservoirs of zoonotic viruses including lyssaviruses (Davis et al., 2013a; Davis et al., 2013b; Albas et al., 2011; Almeida et al., 2011; Almeida et al., 2005), henipaviruses (Roche et al., 2015; Breed et al., 2011; Rahman et al., 2010), coronaviruses (Anthony et al., 2017; Chen et al., 2016; Anindita et al., 2015; Annan et al., 2013; Anthony et al., 2013), picornaviruses (Wu et al., 2012; Lau et al., 2011), and ebola virus(Leroy et al., 2009; Leroy et al., 2005). Because of this, many of the researches focus on isolating viruses from bats.

In the present protocol, samples from bats such as blood, serum, or tissue are homogenized and filtered before inoculation to cell lines. The cell culture was then observed for a few days to weeks and passaged for five times, and discarded if no obvious visual CPE was observed. However, not all viruses show CPE (Papafragkou et al., 2014). In this case, it is highly possible that many important samples, that may have contained a noncytopathic virus, have been discarded and not analyzed. Thus, an alternative to conventional morphology-based CPE is important in viral isolation and detection.

Virus production is expensive and could consume a third of the host's energy (Mahmoudabadi et al., 2017). The intracellular ATP, a major energy currency of the cell, is therefore highly affected in the presence of the virus and could therefore be used as an indicator of viral infection. The ATP can be measured real-time using the recently invented FRET-based ATeam probe (Imamura et al., 2009) which has been used by many studies. However, the use of ATeam for CPE detection and viral isolation has not yet been developed. In this study, the author investigated the early

signs of CPE in virally infected cells through ATP measurement using ATeam technology (ATP-based CPE), and determine the time of ATP-based CPE detection.

## Materials and Methods

*Cells and viruses*

The viruses used in this study, Encephalomyocarditis virus (EMCV) strain NIID-NU1 subgroup 1A (Accession #LC508268), and the Japanese encephalitis virus (JEV, JEV/sw/Chiba/88/2002), were previously isolated and propagated in Vero 9013 cells (JCRB number; JCRB9013) purchased from Human Science Research Resource Bank (HSRRB, Japan), while the Bovine Viral Diarrhea Virus 1 No. 12 (BVDV) (Kishimoto et al., 2017) was propagated in Madin Darby bovine kidney (MDBK) cells in DMEM with 10% fetal bovine serum at 37°C and stored at -80°C until use. All cell lines including baby hamster kidney (BHK-21), and Platinum-E (Plat-E) cells were propagated in DMEM supplemented with 10% fetal bovine serum (FBS) and L-glutamine in the presence of 100 units/ml of penicillin and 100 mg/ml of streptomycin. The Plat-E cells were a kind gift from Dr. Toshio Kitamura (Institute of Medical Science, University of Tokyo) (Morita et al., 2000).

*Plaque assay for EMCV and JEV titration*

The viruses were serially diluted (0.2ml) in DMEM with 2% FBS and were inoculated to ~ 900,000 BHK-21 cells in 6-well plates. The viruses were allowed to adsorb for 1.5 h and then an agarose overlay of 2.4% Seaplaque agar in DMEM with 2% FBS was added to the monolayers. After 30 min at room temperature, the plates were incubated at 37°C, 5% CO2 and > 90% relative humidity. After 1 day for EMCV or 3 days for JEV, 1 ml of 10% formalin was added per well and incubated for 2 h at room temperature. The wells were then washed with PBS until gel is removed, and cells

were stained with 0.1% of crystal violet for 1 min. The excess stain was washed off with PBS (pH 7.2), air-dried, and the number of plaques were evaluated.

*Plasmid construction and transfection*

The ATeam plasmid used in this study was constructed by double digestion with BamH1 and EcoR1 from ATeam 1.03-nD/nA/pcDNA3 (Addgene plasmid 51958). The obtained ATeam probe fragment was then inserted into the BamHI/EcoR1 site of pMXs-IRES-puro (Cell Biolabs Inc., San Diego, CA, USA) to generate pMXs-ATeam-IRES-puro. Plasmid transfection was performed using a retrovirus-mediated gene transfer system. To generate ATeam expressing retroviral vectors, the pMXs-ATeam-IRES-puro was transfected into the Plat-E cells. After 2 days, the supernatant was collected and transduced into the BHK-21 cells using ViroMag® following manufacturer's instructions. Two days post-transduction, BHK-21 cells containing pMXs-ATeam-IRES-puro (BHK-ATeam) were selected with the same medium containing 8 μg/ml Puromycin.

*Viral infection and cell fixation*

One day prior to viral infection, the BHK-ATeam were seeded onto 4-compartment, 35 mm Cellview$^{TM}$ glass-bottomed dishes (Greiner Bio-One Co. Ltd., Tokyo, Japan). Approximately 50,000 cells were seeded onto each 1.9 $cm^2$ compartment and after 1 day, the cells were infected with the virus at MOI 1, 3, and 5 pfu/ml for EMCV and JEV, or genome copy/ul for BVDV. After 3, 6, 9, 16, and 24 h of incubation, the medium was removed and washed one time with PBS before adding

4% PFA until ready for observation under confocal microscope. To adhere to biosafety regulations, for laboratories less than BSL-2, the cells were fixed prior to imaging.

*Imaging and analysis*

The cells were excited by a 405-nm laser diode, and CFP and Venus were detected at 480–500 nm and 515–615 nm wavelength ranges, respectively. The images were obtained using an Olympus Fluoview FV1000 confocal microscope with an oil-immersion UPLSAPO objective (NA=1.35) (Carl Zeiss, Jena, Germany). Using the FRET application, fluorescence intensities from CFP and Venus channels were obtained from individual fluorescence-expressing cells. All image analyses were performed using ImageJ (National Institutes of Health, MD, USA).

Fluorescence intensities of cytoplasmic areas in cells were obtained manually by tracing the cytoplasm of the cells using drawing tablet (Wacom Co., Ltd., Saitama, Japan). The corrected cell fluorescence (CTCF) from Venus and CFP channel was then calculated using the formula: Integrated Density – (Area of selected cell) * (Mean fluorescence of background readings). Each Venus/CFP emission ratio was calculated by dividing the CTCF of a Venus image with a CFP image.

To investigate the relationship of ATP with Venus/CFP ratios, BHK-ATeam cells were permeabilized with 5µg/ml digitonin in buffer B (20 mM HEPES-KOH [pH 7.7], 110 mM potassium acetate, 2 mM magnesium acetate, 1 mM EGTA, and 2 mM dithiothreitol) for 5 min at room temperature. The reaction was stopped by washing the cells with buffer B thrice, followed by addition of known concentrations of ATP in buffer B. Plots were fitted with Hill equations with a fixed Hill coefficient of 1.7; $R= (R_{max} - R_{min})x[ATP]^2/([ATP]^2+Kd^2)+R_{min}$, where $R_{max}$ and $R_{min}$ are the maximum

and minimum fluorescence ratios, respectively, and *Kd* is the apparent dissociation constant.

*Nucleic acid extraction and quantitative RT- PCR*

Nucleic acid extraction was performed using ISOGEN II (Nippon Gene, Japan and RNA clean-up was done using RNeasy Mini Kit (Qiagen, Hilden, Germany) and the first strand cDNA synthesis was prepared with ReverTra Ace® qPCR RT Master Mix (Toyobo Co., Ltd., Osaka, Japan). The list of primers and probes used in this study is shown in Table 1-2.

A LightCycler Nano (Roche 120 Diagnostics GmbH, Mannheim, Germany) was used for all qRT-PCRs performed in this study. Thunderbird®SYBR®qPCR Mix (Toyobo Co., Ltd., Osaka, Japan) was used with the following thermal cycling conditions: 95°C for 30 s, followed by 40 cycles of 95°C for 15 s, 55°C for 30 s and 72°C for 30 s.

Titration of the BVDV for infection was done by qPCR as previously described (Rahpaya et al., 2018; Kishimoto et al., 2017; Tsuchiaka et al., 2015) except for EMCV and JEV, which were titrated using a plaque assay.

*Statistical Analysis*

Data are shown as the mean ± S.D., and statistical significance was determined by Student's t-test and Dunnett's test, with $p < 0.01$ is considered statistically significant.

**Results**

The experiment workflow of this study is shown in Figure 1-1. This study uses ATeam technology in visualizing ATP level in viral-infected cells as an indicator of an early sign of CPE, and the mechanism is shown in Figure 1-2. To adhere to biosafety regulations, for laboratories less than BSL-2, the cells must be fixed to inactivate the virus before imaging in microscopy our room. Thus, in this study, virus-infected cells were fixed with 4% PFA to inactivate the viruses prior to imaging. To determine if the measurement of ATP levels in fixed cells is possible, uninfected live and fixed cells were compared. The fixed cells have a significantly lower ATP value compared to the live cells, but the ATP level remains detectable (Fig. 1-4A). To test if the ATeam probe expressed by BHK-ATeam cells is responsive to the varying concentrations of ATP, the BHK-ATeam cells were permeabilized with digitonin, fixed, and treated with different concentrations of ATP. Figure 1-3 shows that the Venus/CFP ratio indeed increases as the ATP concentration is increased.

Figure 1-4 B-D shows the Venus/CFP ratio obtained in BVDV, EMCV, and JEV infected BHK-ATeam cells. Results showed that all the viral infected cells exhibit a significantly lower ratio compared to the mock-infected cells in as early as 3 h. In MOI-5 BVDV-infected showed a significantly lower Venus/CFP ratio compared to the mock control cells (Fig. 1-4B). At 6 h, the cells infected with MOI-1, 3, and 5 showed a significantly higher ratio; while at 16 h and 24 h, only MOI-5 showed a significantly higher ratio while other concentrations showed no significant difference. The JEV-infected cells showed a significantly lower ratio at 3 h with MOI-5, at 6 h with MO-1 and 5, and at 16 and 24 h with MOI-1, 3, and 5 (Fig. 1-4C). The EMCV-

infected cells also showed a significantly lower ATP value than the mock control at 3 h with MOI-1 and 5 but not at 6 h (Fig. 1-4D). Most of the EMCV-infected cells were dead by 16 h; thus, no datum was obtained at this incubation time.

To determine if viral infection have occurred in the BHK-ATeam cells, qPCR of the viral-infected cells was done. Table 1-1 shows the qPCR results from BVDV, JEV, and EMCV at MOI-5. The BVDV, JEV, and EMCV shows high infectivity at 3 h. The JEV infectivity is higher at day 1 although EMCV could not be measured due to the death of all cells at 24 h post-infection. In contrast, the BVDV showed low amounts of virus at day 6 post-infection with Cq above 30. Among these viruses, only BVDV does not exhibit morphology-based CPE while EMCV showed morphology-based CPE at 16 h post-infection and JEV at 3 days post-infection as shown in Figure 1-5.

**Discussion**

This study used ATeam technology to detect the early signs of viral infection. The recombinant ATeam probe responded well to ATP in a dose-dependent manner (Fig. 1-3). The lowest Venus/CFP ratio is approximately 1.4 for no ATP, which means that it measured the existing ATP level of the cells and increases with the addition of higher ATP concentration. The possibility of measuring the Venus/CFP ratio in fixed cells was confirmed, although the value is significantly lower than that of the live cells (Fig 1-4A). This suggests that the attachment of ATP to the ATeam probe was conserved and therefore, the ATP level in fixed cells can be measured. However, the conformation of the Ɛ subunit may have been affected during fixation resulting in a lower Venus/CFP ratio. Nevertheless, the value is measurable and thus, fixed cells were used in this study.

The BHK-ATeam cells infected with BVDV, EMCV, and JEV showed a significantly lower ratio compared to mock samples as early as 3 h (Fig. 1-4 B-D). This indicates a high consumption of ATP during the early phase of infection. This decrease in cytoplasmic ATP has also been observed in other RNA viruses such as HCV (Ando et al., 2012) and influenza virus (Maruyama et al., 2018; Ritter et al., 2010). However, the non-cytopathic BVDV showed a higher Venus/CFP ratio in infected cells at 6 h until 24 h post-infection. The initial cellular response to a stressful stimulus involves protecting the cell against insult and promoting recovery (Fulda et al., 2010). Thus, it is highly likely that the cells have responded to the viral presence by increasing ATP generation while viral replication rates remained the same or lower. This is supported by the qPCR result wherein BVDV showed high numbers at 3 h, but low numbers at 6 days post-infection (Table 1-1). This low viral numbers of BVDV

after few days of infection also explains the noncytopathic nature of this virus. It is possible that the replication of BVDV continues at a regulated rate.

The JEV-infected cells continued to show a significantly lower ratio compared to mock samples indicating a higher rate of ATP consumption by this cytopathic virus compared to the rate of ATP generation by cells throughout the infection. In contrast, the EMCV-infected cells showed no significant difference in Venus/CFP ratio at 6 h post-infection. It is likely that the cells have increased ATP generation to compensate for the consumption leading to the generation-consumption equilibrium. However, at 12 h, the EMCV-infected cells died, owing to the oxidative stress caused by the virus in cells during infection (Anand and Tikoo, 2013). The ATP in these RNA viruses is quickly consumed as many steps in the viral life cycle require high energy phosphoryl groups (Ando et al., 2012), such as the formation of the preinitiation complex for *de novo* RNA synthesis by RdRp of flaviviruses (Nomaguchi et al., 2003), ATP-dependent transcriptional initiation and RNA replication by influenza virus RdRp (Vreede et al., 2008; Klumpp et al., 1998), and assembly and/or release of viral structural proteins possibly via interaction with ATP-dependent chaperones (Li et al., 2008; Gurer et al., 2005).

The replication of BVDV, JEV, and EMCV was confirmed by qPCR (Table 1-1). The low replication of BVDV explains the increase in intracellular ATP at 6 h to 24 h post-infection, while the high replication of JEV and EMCV explains the continued low ratio of JEV-infected cells until 24-h post-infection and the death of EMCV-infected cells beyond 6-h post-infection. Under light microscopy, morphology-based CPE usually appears at 16h for EMCV, on day 3 for JEV, while BVDV is noncytopathic (Fig. 1-5); however, the ATP-based CPE using ATeam

technology is already evident at 3 h. This indicates that the ATeam technology is not only an early marker for the CPE but also a novel indicator for the infected cells without morphology-based CPE.

**Figures and Tables**

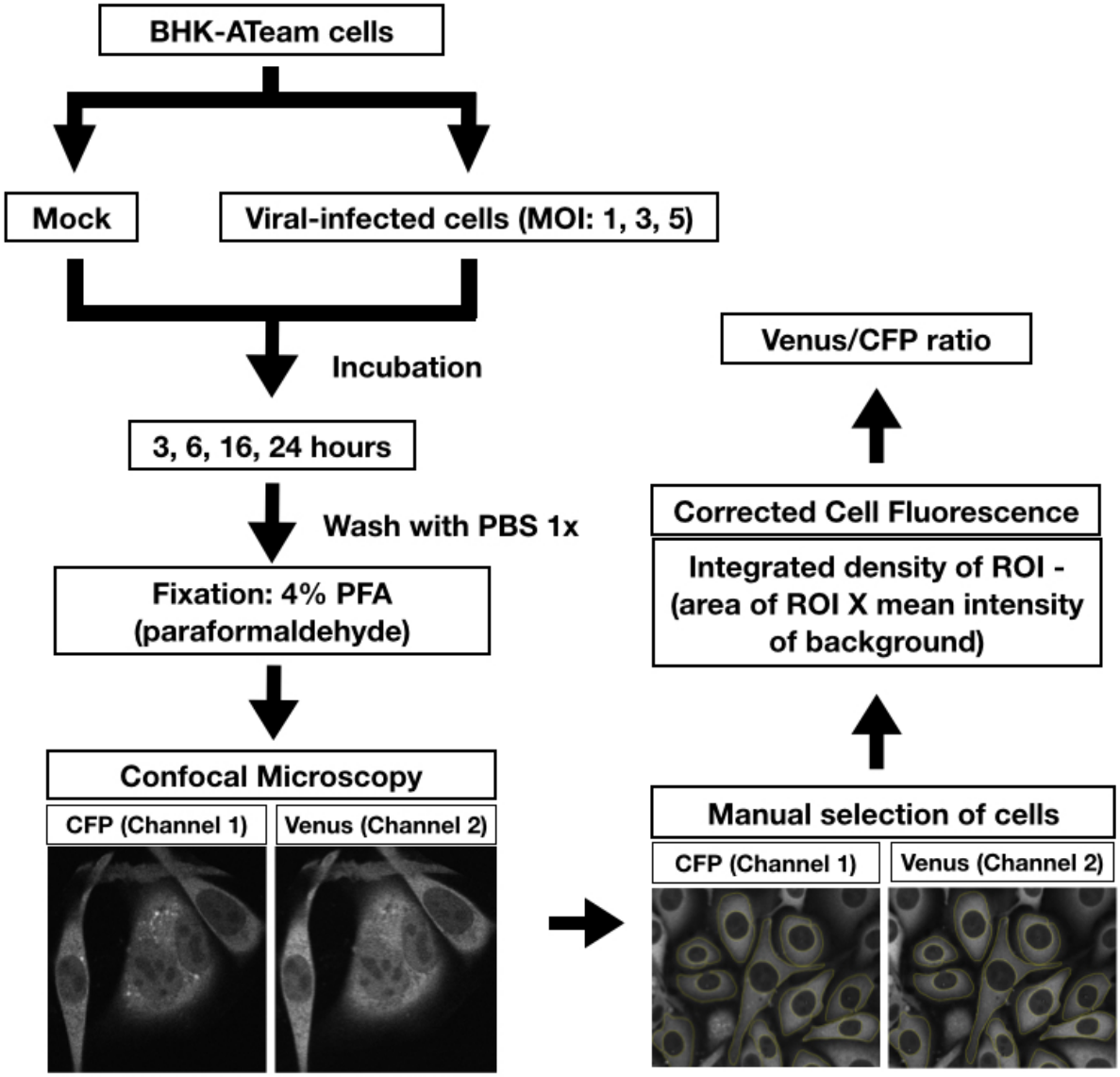


Figure 1-1. The experiment workflow of Chapter 1. The BHK-Ateam cells were either mock-infected or viral-infected with MOI of 1, 3, or 5 pfu/ml or viral copy number/µl. the cells were incubated for 3, 6, 16, or 24 hours and fixed with 4% PFA for 10 min. the fixed cells were then subjected to confocal microscopy where images from Venus and CFP channel were obtained. The images were then analyzed in ImageJ where cells were manually selected followed by computation of corrected cell fluorescence and subsequent Venus/CFP calculation per cell.

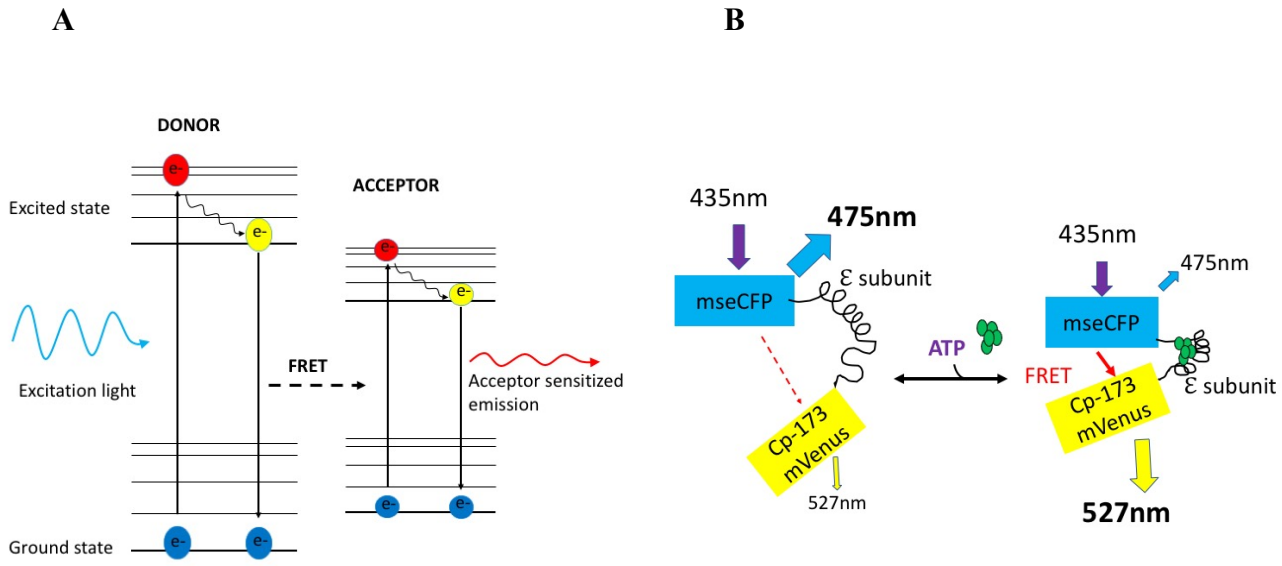


Figure 1-2. FRET-based ATP probe, ATeam. (A) Jablonski diagram of FRET technique modified from Hochreiter et al. (2019). The photon is absorbed by the fluorophore causing excitation of the electron from the ground state to a higher energy state. After a few nanoseconds, the electron will return to its ground state by releasing their stored energy in an emitted photon or the energy, which can be transferred to an electron of a nearby fluorophore. This will lead to excitation of the electron and fluorescence of the acceptor. (B) Schematic diagram of the ATeam probe modified from Imamura et al. (2009). The mseCFP and cp173-mVenus were bonded by Ɛ subunit of *Bacillus subtilis* FoF1 ATP synthase. In the absence of ATP, the flexible and stretched conformation of the Ɛ subunit separates the two fluorophores, causing low FRET efficiency. In the presence of ATP, the ATP binds to the Ɛ subunit causing retraction and drawing the two fluorophores close to each other. This results in the transfer of energy to the cp173 Venus, increasing the FRET efficiency.

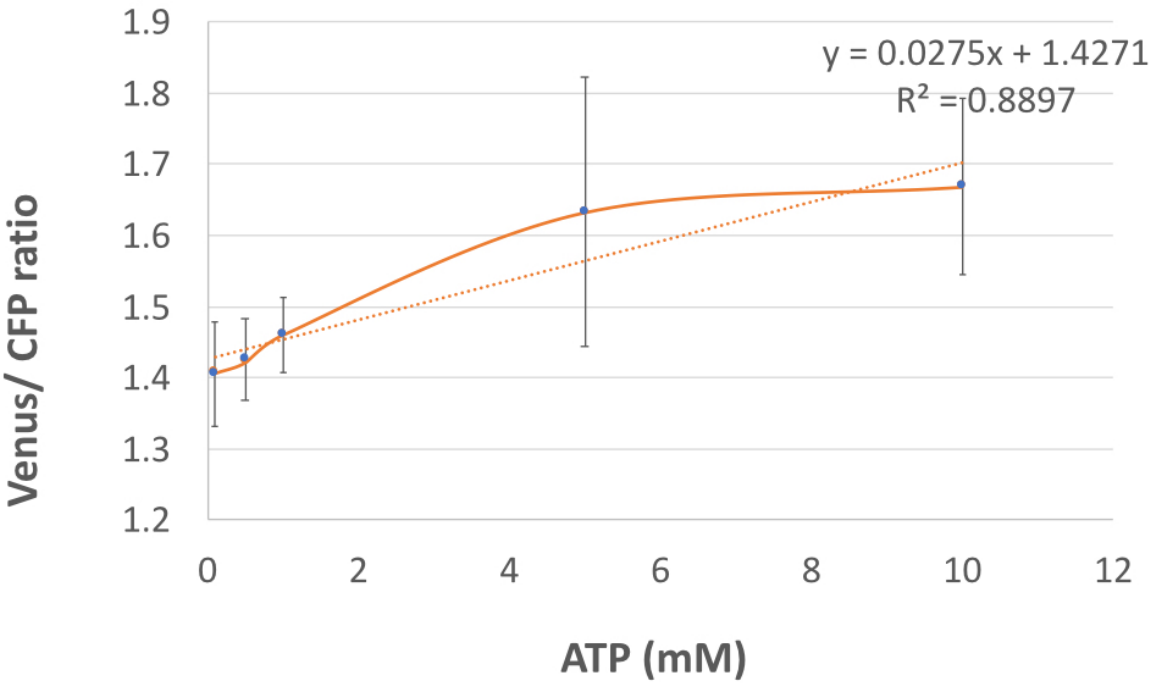


Figure 1-3. The response of ATeam to the varying concentrations of ATP. Each point represents mean with SD of at least 60 independent cells. Plots were fitted with Hill equations with a fixed Hill coefficient of 2; $R= (R_{max} - R_{min})x[ATP]^2/([ATP]^2+Kd^2)+R_{min}$, where $R_{max}$ and $R_{min}$ are the maximum and minimum fluorescence ratios, respectively. *Kd* is the apparent dissociation constant.

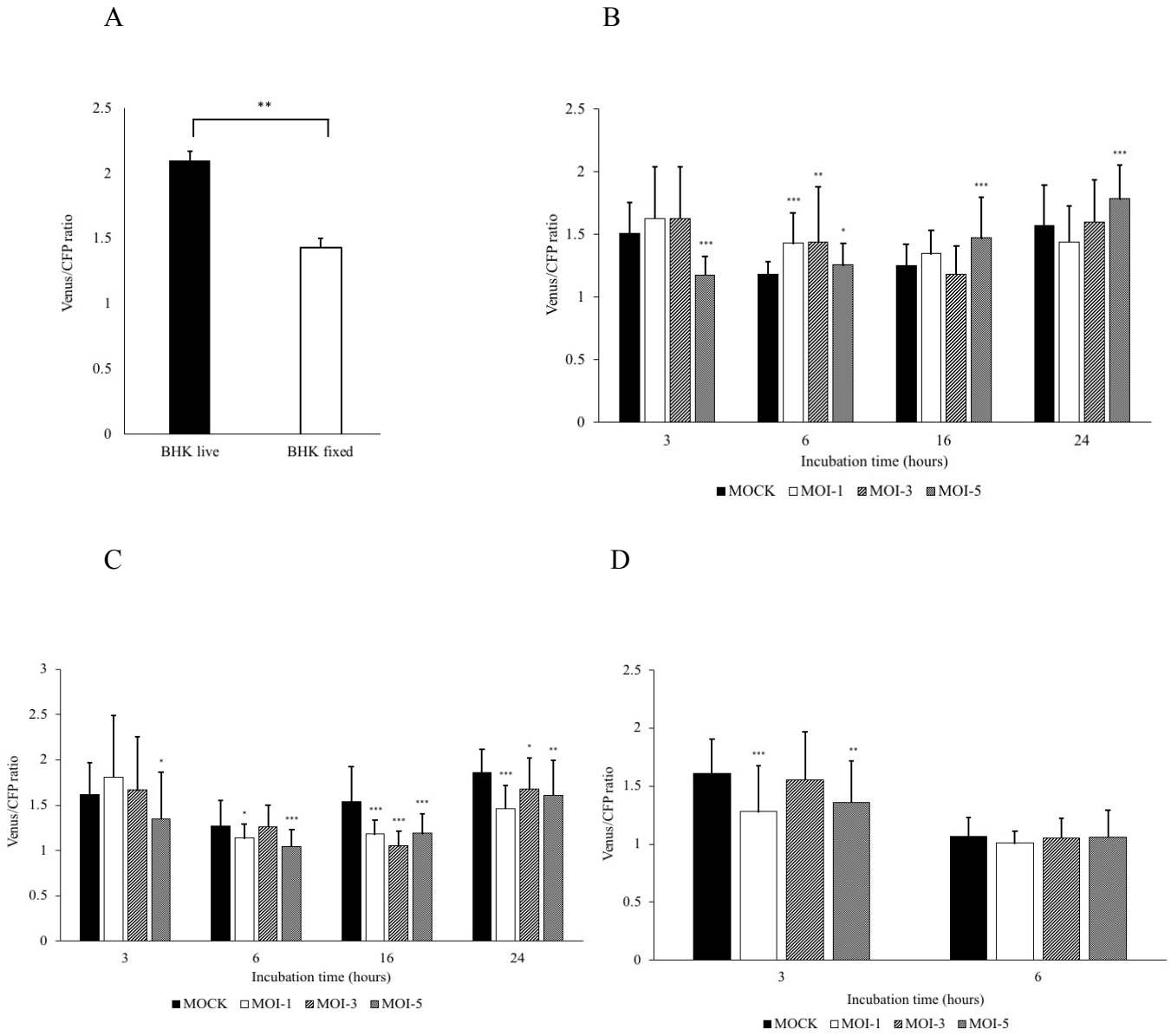


Figure 1-4. Venus/CFP ratio in manually selected BHK-ATeam cells. (A) BHK-ATeam fixed cells. (B)BVDV-infected cells. (C) JEV-infected cells. (D) EMCV-infected cells. The BHK-ATeam cells were inoculated with different concentrations of the virus (MOI-1, 3, or 5), formalin-fixed for 10 minutes, and the Venus/CFP emission ratios were calculated from images of Venus and CFP channels in individual cells at different time points. Data are shown as the mean ± S.D. of at least 50 individual cells, and statistical significance was determined byStudent's t-test between BHK live and BHK fixed cells, and by Dunnett's test between various MOI versus the control (* $p < 0.01$, ** $p < 0.001$, *** $p < 0.0001$). All data are expressed in means with error bars indicating S.D.

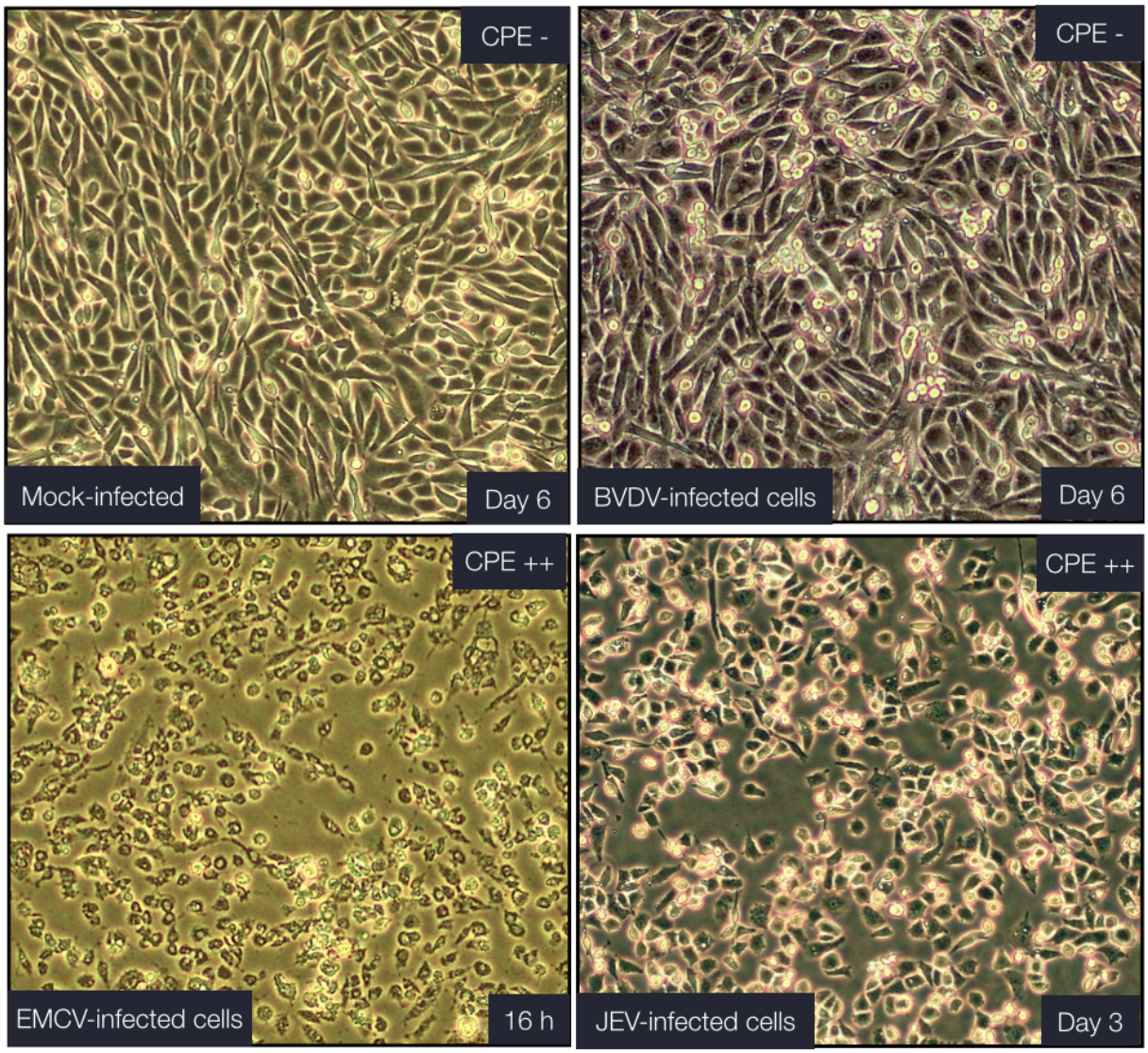


Figure 1-5. The viral-infected BHK-Ateam cells showing cytopathic and non-cytopathic viruses. The bovine viral diarrhea (BVDV) showed no CPE, the encephalomyocarditis virus EMCV showed CPE at 16h post-infection, and Japanese encephalitis virus (JEV) showed CPE at day 3 post-infection

Table 1-1. The qPCR result of BVDV, EMCV, and JEV infected BHK-ATeam cells.

| Virus name | Incubation time | Cq |
|---|---|---|
| Bovine Viral Diarrhea Virus | 3 hours | 24.96 |
| | 6 days | 32.67 |
| | Negative Control | 40.27 |
| Japanese Encephalitis Virus | 3 hours | 19.94 |
| | 1 day | 14.14 |
| | Negative Control | – |
| Encephalomyocarditis Virus | 3 hours | 13.70 |
| | Negative Control | 34.96 |

Cq: Cycle number; –: negative

Table 1-2. Primers and Probes used in this study

| **Virus name** | | **Primer/Probe sequence 5'-3' (FAM/TAMRA)** |
|---|---|---|
| Bovine viral diarrhea virus | F | GGGNAGTCGTCARTGGTTCG |
| | R | GTGCCATGTACAGCAGAGWTTTT |
| | P | CCAYGTGGACGAGGGCAYGC |
| Encephalomyocarditis virus | F | ATTCCACCTCCTCAGACAAGA |
| | R | AGCTAGCAATGGAAGCATAT |
| Japanese encephalitis virus | F | TCGCCCATCACCAGTGCGAG |
| | R | TTGATAACATCCACTTG |

F: forward, R: reverse, P: probe

# Chapter 2:

# Automatic method for ATeam analysis

## Introduction

Chapter 1 has revealed that Ateam technology detects ATP-based CPE as early as 3 hours. Thus, this technology is highly useful in viral isolation studies. However, the manual selection of cells and subsequent calculation of Venus/CFP ratio in Chapter 1 requires a lot of time and sometimes, human bias in selection may occur. To eliminate this human bias, the Study 2 developed a software program that is more rapid, more convenient, and automatically selects cells and calculate FRET.

The newly-developed program in this study was named Boomerang Catcher (BC). It is an ImageJ and Python programs set that automatically analyses FRET in cells available at this link: URL: https://github.com/ishibaki/boomerang_catcher. The algorithm of this program performs the following major steps: (1) increase the signal/noise ratio, (2) smoothen and detect the cell edge, (3) eliminate too large area such as overlapping cells, (4) eliminate too small area that could only be noise, (5) obtain the mean intensity of the cytoplasm of the cell, and (6) calculate the Venus/CFP ratio of the cells. This algorithm was developed based on the 50 cells from 10 images obtained by confocal microscopy.

In this study, the author investigated the ATP level of viral-infected cells using the newly-developed program BC.

## Materials and Methods

*Cells and viruses*

The viruses used in this study were the Bovine Parainfluenza virus 3 BN-1 (BPIV3)(Kishimoto et al., 2017), Bovine Coronavirus (BCV), Bovine Enterovirus (BEV, BEV Ho12/Bos taurus/JPN/2014), Infectious Bovine Rhinotracheitis Virus (IBR) (Tsuchiaka et al., 2015), Porcine teschovirus 15 JPN/Ishi-Ka2/2015/G (PTV) (Oba et al., 2018), and Akabane virus Ja GAR 39. The baby hamster kidney (BHK-21) was propagated in DMEM supplemented with 10% fetal bovine serum (FBS) and L-glutamine in the presence of 100 units/ml of penicillin and 100 mg/ml of streptomycin.

*Viral infection and cell fixation*

One day prior to viral infection, the BHK-ATeam were seeded onto 4-compartment, 35 mm Cellview$^{TM}$ glass-bottomed dishes (Greiner Bio-One Co. Ltd., Tokyo, Japan). Approximately 50,000 cells were seeded onto each 1.9 $cm^2$ compartment and after 1 day, the cells were infected with the virus at MOI 0.25, 0.75, and 1.25 genome copy/ul. After 3 h of incubation, the medium was removed and washed one time with PBS before adding 4% PFA until ready for observation under confocal microscope. To adhere to biosafety regulations, for laboratories less than BSL-2, the cells were fixed prior to imaging.

*Automatic selection of cells and Venus/CFP ratio using the newly developed program*

The images captured in confocal microscopy were then subjected to boomerang catcher (BC), the ImageJ & Python programs set to analyze FRET in viral-infected cells developed in this study, available at this link (URL: https://github.com/ishibaki/boomerang_catcher) (Fig. 2-3 and 2-4). The algorithm was designed to subtract the background and enhance the contrast from channel-2 (Venus) images, followed by the enhancement of contrast until 0.3% of pixels were saturated. The Gaussian Blur (sigma =4) was then applied, followed with the threshold by minimum method to detect the cell body without the nucleus (filter 1) (Fig. 2-2). Cells with an area of 50-500 $\mu m^2$ were then selected. A threshold image produced from the previous step was duplicated wherein a threshold set by the Otsu method, a method that finds an optimal threshold based on the observed distribution of pixels (Khushbu and Vats, 2017), was applied to detect the cell body and nucleus (filter 2). Cells with an area of 50-800 $\mu m^2$ were selected. To generate a nuclear mask (filter 3), the inverted filter 1 and filter 2 were multiplied. The average intensity of channel-1 and channel-2 from filters 1 (Data1) and 3 (Data3) were calculated. The mean intensity of each channel was then calculated using the formula: ((Area of Data 1) * (Mean Intensity of Data 1) - ((Area of Data 2) * (Mean Intensity of Data 2))) / ((Area of Data 1) - (Area of Data 2)). The Venus/CFP ratio was then acquired using the formula: (Mean Intensity of Channel-2) / (Mean Intensity of Channel-1).

*Nucleic acid extraction and quantitative PCR*

The viral nucleic acid was prepared using High Pure™ Viral Nucleic Acid Kit (Roche, Basel, Switzerland). A LightCycler Nano (Roche 120 Diagnostics GmbH, Mannheim, Germany) was used for all qRT-PCRs performed in this study. A one step PrimeScript RT-PCR Kit (Perfect Real time) (TaKaRa Bio, Otsu, Japan) was used for the amplification of extracts from RNA/DNA viruses. Thermal cycling conditions were as follows: 45°C for 5 min and 95°C for 30 s, followed by 40 cycles of 95°C for 10 s, 55°C for 20 s and 72°C for 20 s. GoTaq 1-step RT-qPCR system (Promega, WI, USA) was used for PTV-ka2 virus with the following thermal cycling conditions: 42°C for 15 min and 95°C for 10 s, followed by 40 cycles of 95°C for 10 s, 50°C for 30 s and 72°C for 30 s. Titration of the viruses for infection were done by qPCR as previously described (Rahpaya et al., 2018; Kishimoto et al., 2017; Tsuchiaka et al., 2015). The list of primers and probes used in this study is shown in Table 2-3.

*Statistical Analysis*

Data are shown as the mean ± S.D., and statistical significance was determined by Dunnett's test, with $p < 0.01$ is considered statistically significant.

**Results**

The experiment workflow of this study is shown in Figure 2-1. In this study, we developed a BC program which automatically analyzes automatically the FRET in viral infected BHK-ATeam cells (Fig. 2-2, 3, & 4). This program was devised to evaluate the Venus/CFP ratio. Subsequently, it detects the cell body and calculates the mean intensity of the cell body in CFP and Venus channels, followed by the calculation of the Venus/CFP ratio. The BHK-ATeam cells were infected with Akabane virus, BCV, BEV, BPIV3, IBR, and PTV-ka2 for 3 h, fixed and examined under confocal microscopy, and the Venus/CFP ratio was obtained using the BC program. Table 2-1 shows the Venus/CFP ratio of infected BHK-ATeam cells by the selected virus for 3 h, using the developed program. More than 60 cells per group were selected by the program, and results revealed that all the viral-infected cells showed significantly different Venus/CFP ratio compared to the mock control. The BCV, BEV with MOI-0.25 and 0.75 viral copy number/ul, BPIV3, and IBR infected cells exhibited significantly higher ratio compared to the mock, while the PTV-ka2 with MOI- 0.75 and 1.25 viral copy number/ul, and Akabane virus with MOI-0.25 viral copy number/ul showed significantly lower value. Figure 2-5 shows that the morphology-based CPE of Akabane virus, BCV, and BPIV3 showed morphology-based CPE at day 3, day 5, and day 6 post-infection, respectively, the BEV showed mild morphology-based CPE at day 6 post-infection, while IBR and PTV-ka2 did not show signs of morphology-based CPE.

To determine the infectivity of these viruses in the BHK-ATeam cells, qPCR was also performed at MOI 1.25 viral copy number/ul. Results revealed that at 3h post-infection, viral numbers are low with Cq values of 28.03 in PTV-ka2 to 35.16 in BPIV3,

while the Akabane virus is undetectable at this period (Table 2-2). However, after 6 days (or 4 days for Akabane virus) post-infection, the qPCR data showed a higher amount of virus with Cq values of 15.61 in BPIV3 to 26.77 in PTV-ka2.

## Discussion

To make the selection of cells and measurement of the Venus/CFP ratio more efficient, rapid, and objective; an ImageJ and Python program was created in this study. The program set was used to analyze the Venus/CFP ratio of the infected cells by the selected viruses for 3 h. All the viruses caused a significant difference in the Venus/CFP ratio although not the same pattern (Table 2-1). PTV-ka2 and Akabane viruses showed a significantly lower ratio while other viruses showed a significantly higher ratio as compared to mock controls. This result of PTV-ka2 and Akabane virus-infected cells is similar to what was observed in BVDV, EMCV, and JEV infected cells and in previously reported RNA viruses such as HCV, influenza virus, and dengue virus (Maruyama et al., 2018; Ando et al., 2012; Ritter et al., 2010; El-Bacha et al., 2007). The other viruses, namely BCV, BEV, BPIV3, and IBR showed a significantly higher ratio than mock-infected cells. This result is similar to previously reported vaccinia virus (Chang et al., 2009), HCMV (Munger et al., 2006), baculovirus (Olejnik et al., 2004), and avian reovirus (Chi et al., 2018) where increased in intracellular ATP was observed because of the upregulation of mitochondrial genes for proteins that are part of the ETC and upregulation of TCA to increase ATP production for virus propagation (Goodwin et al., 2015; Munger et al., 2006).

There were differences of results in MOI observed in viruses. Although the MOI 1.25 viral copy number/ul, the highest MOI, has been observed to be generally significantly different to the mock-infected but is not the case in BEV and Akabane. In BEV, only the MOI 0.25 and 0.75 viral copy number/ul, while in Akabane virus only the MOI 0.25 viral copy number/ul showed significant difference compared to mock. There are two possibilities hypothesized: the high numbers of virus infected

may have caused a more rapid response by the cells through increasing ATP generation leading to a normal ATP level at 3h post-infection; or the high viral numbers may have caused a competition on cellular receptors leading to a delay in viral entry.

The qPCR results of these viruses (Table 2-2) showed low viral numbers at 3 h but have increased after 3-6 days post-infection. Among the viruses tested, the morphology-based CPE usually appears day 3 for Akabane virus, day 5 for BCV, day 6 for BPIV3 and BEV, while IBR and PTV-ka2 showed no morphology-based CPE (Fig. 2-5). Thus, the ATeam system is a fast way to determine ATP-based CPE by a viral infection, which is as early as 3 h when the morphology-based CPE and qPCR are yet to be conclusive.

**Figures and Tables**

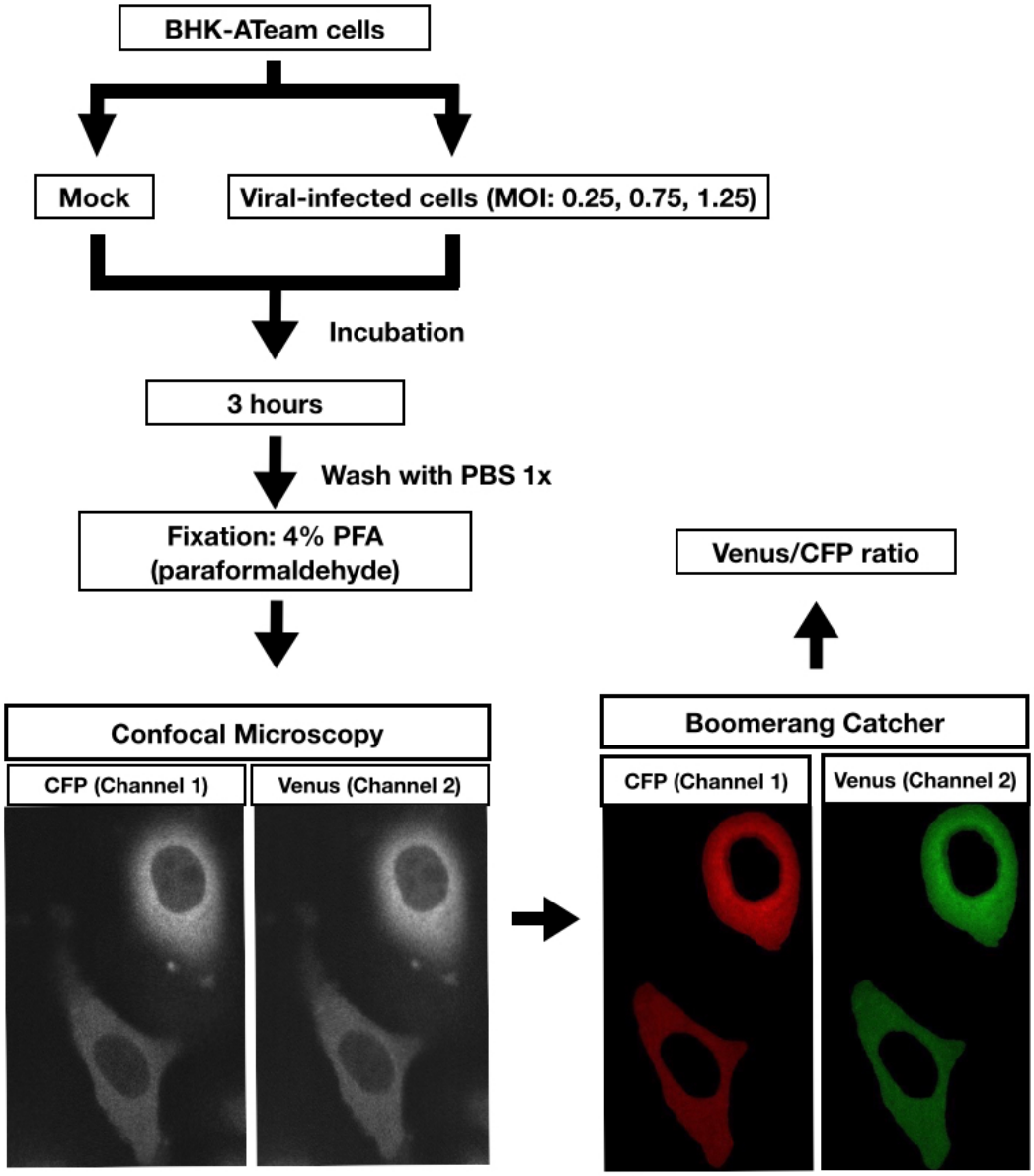


Figure 2-1. the experiment workflow of Chapter 2. The BHK-ATeam cells were either mock-infected or viral-infected with MOI 0.25, 0.75, or 1.25 viral copy number/µl, incubated for 3h, and subsequently fixed with 4% PFA for 10 min. the cells were then examined under confocal microscope where images from Venus and CFP channels were obtained. The images were then automatically analyzed by the Boomerang catcher that automatically generates the Venus/CFP ratio.

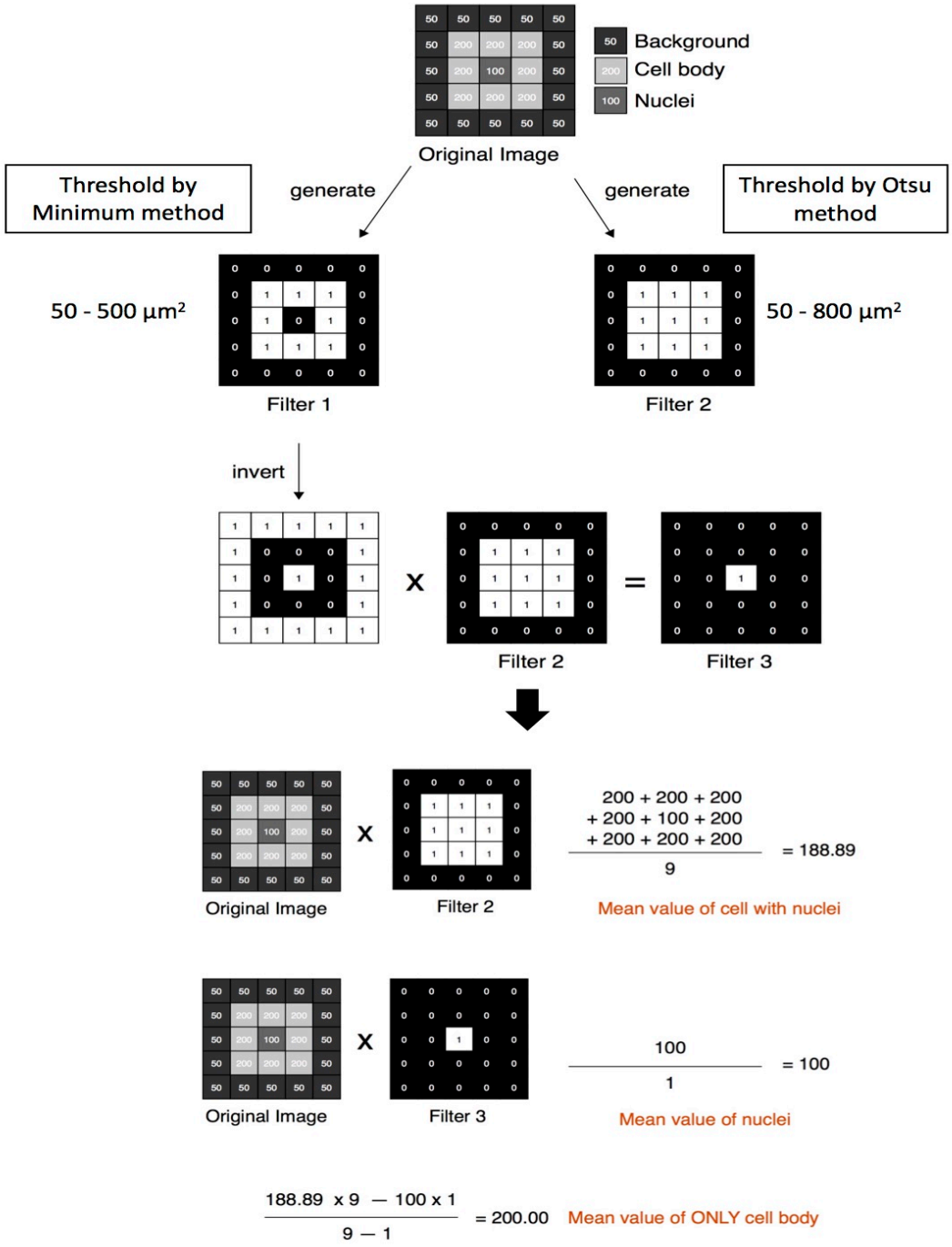


Figure 2-2. The workflow of the developed Image J and Python programs set named Boomerang catcher.

```
rename("img.tif");
run("Set Measurements...", "area mean min centroid center perimeter fit shape stack
display redirect=None decimal=8");
run("Split Channels");
selectWindow("C2-img.tif");
run("Duplicate...", "duplicate");
rename("filter1.tif");
run("Duplicate...", "duplicate");
rename("filter2.tif");
selectWindow("filter1.tif");
run("Subtract Background...", "rolling=50 stack");
run("Enhance Contrast...", "saturated=0.3 normalize equalize process_all");

run("Gaussian Blur...", "sigma=4 stack");
setAutoThreshold("Minimum dark");
run("Analyze Particles...", "size=50.00-500.00 show=Masks exclude clear add
stack");
selectWindow("filter2.tif");
run("Subtract Background...", "rolling=50 stack");
run("Enhance Contrast...", "saturated=0.3 normalize equalize process_all");

run("Gaussian Blur...", "sigma=4 stack");
setAutoThreshold("Minimum dark");
run("Analyze Particles...", "size=50.00-800.00 show=Masks exclude clear include
stack in_situ");
selectWindow("Mask of filter1.tif");
run("Invert",  "stack")
imageCalculator("Multiply create stack", "filter2.tif", "Mask of filter1.tif")
selectWindow("Result of filter2.tif")
setAutoThreshold("Otsu dark");
run("Analyze Particles...", "size=30-350 circularity=0.6-1.00 show=Masks exclude
include add in_situ stack");
run("Set Measurements...", "area mean min centroid center perimeter fit shape stack
display redirect=None decimal=8");
selectWindow("C1-img.tif");
roiManager("Measure");
selectWindow("C2-img.tif");
roiManager("Measure");
selectWindow("C1-img.tif");
imageCalculator("AND stack", "C1-img.tif","filter2.tif");
imageCalculator("Subtract stack", "C1-img.tif","Result of filter2.tif");

selectWindow("C2-img.tif");
imageCalculator("AND stack", "C2-img.tif","filter2.tif");
imageCalculator("Subtract stack", "C2-img.tif","Result of filter2.tif");

selectWindow("Mask of filter1.tif");
run("Close");
selectWindow("ROI Manager")
run("Close");
selectWindow("filter2.tif")
run("Close");
selectWindow("Result of filter2.tif")
run("Close");
```

Figure 2-3. Boomerang Catcher code

```
df = pd.read_csv('Results.csv', index_col=0)
df_ch1 = df[df['Label'].str.startswith('C1')]
df_ch2 = df[df['Label'].str.startswith('C2')]
diff = np.array(df_ch1['Slice'].iloc[1:]) - np.array(df_ch1['Slice'].iloc[:-1])

delimiting_point = np.where(diff < 0)[0][0] + 1

df_ch1_cellbody = df_ch1.iloc[0:delimiting_point, :]
df_ch1_nuclear = df_ch1.iloc[delimiting_point:, :]
df_ch2_cellbody = df_ch2.iloc[0:delimiting_point, :]
df_ch2_nuclear = df_ch2.iloc[delimiting_point:, :]

for nuc_index in df_ch1_nuclear.index:
    x, y, z= df_ch1_nuclear.loc[nuc_index, ["X", "Y", "Slice"]]
    area_nuc, mean_nuc = df_ch1_nuclear.loc[nuc_index, ["Area", "Mean"]]
    same_slice = df_ch1_cellbody[df_ch1_cellbody["Slice"] == z]
    dx2 = np.square(same_slice["X"] - x)
    dy2 = np.square(same_slice["Y"] - y)
    coord_index = np.argmin(np.sqrt(dx2 + dy2))

    area_cell, mean_cell = df_ch1_cellbody.loc[coord_index, ["Area", "Mean"]]
    mean_cell = ((area_cell * mean_cell) - (area_nuc * mean_nuc))\
                /(area_cell - area_nuc)
    df_ch1_cellbody.loc[coord_index, "Mean"] = mean_cell
    df_ch1_cellbody.loc[coord_index, "Area"] = area_cell - area_nuc

for nuc_index in df_ch2_nuclear.index:
    x, y, z= df_ch2_nuclear.loc[nuc_index, ["X", "Y", "Slice"]]
    area_nuc, mean_nuc = df_ch2_nuclear.loc[nuc_index, ["Area", "Mean"]]
    same_slice = df_ch2_cellbody[df_ch2_cellbody["Slice"] == z]
    dx2 = np.square(same_slice["X"] - x)
    dy2 = np.square(same_slice["Y"] - y)
    coord_index = np.argmin(np.sqrt(dx2 + dy2))
     area_cell, mean_cell = df_ch2_cellbody.loc[coord_index, ["Area", "Mean"]]
    mean_cell = ((area_cell * mean_cell) - (area_nuc * mean_nuc))\
                /(area_cell - area_nuc)
    df_ch2_cellbody.loc[coord_index, "Mean"] = mean_cell
    df_ch2_cellbody.loc[coord_index, "Area"] = area_cell - area_nuc

   ch2_ch1_ratio = np.array(df_ch2_cellbody["Mean"])\
                /np.array(df_ch1_cellbody["Mean"])

df_ch1_cellbody = df_ch1_cellbody.rename(columns={"Mean": "Ch1_Mean"})
df_ch1_cellbody["Ch2_Mean"] = np.array(df_ch2_cellbody["Mean"])
df_ch1_cellbody["Ch2/Ch1-Ratio"] = ch2_ch1_ratio

out = df_ch1_cellbody.loc[:, ['Label', 'Area', 'Ch1_Mean', 'Ch2_Mean',
                              'Ch2/Ch1-Ratio', 'Min', 'Max', 'X', 'Y',
                              'XM', 'YM', 'Perim.', 'Major', 'Minor', 'Angle',
                              'Circ.', 'Slice', 'AR', 'Round', 'Solidity']]

out.to_csv("out.csv")
```

Fig. 2-4. Python program code for calculating Venus/CFP ratio

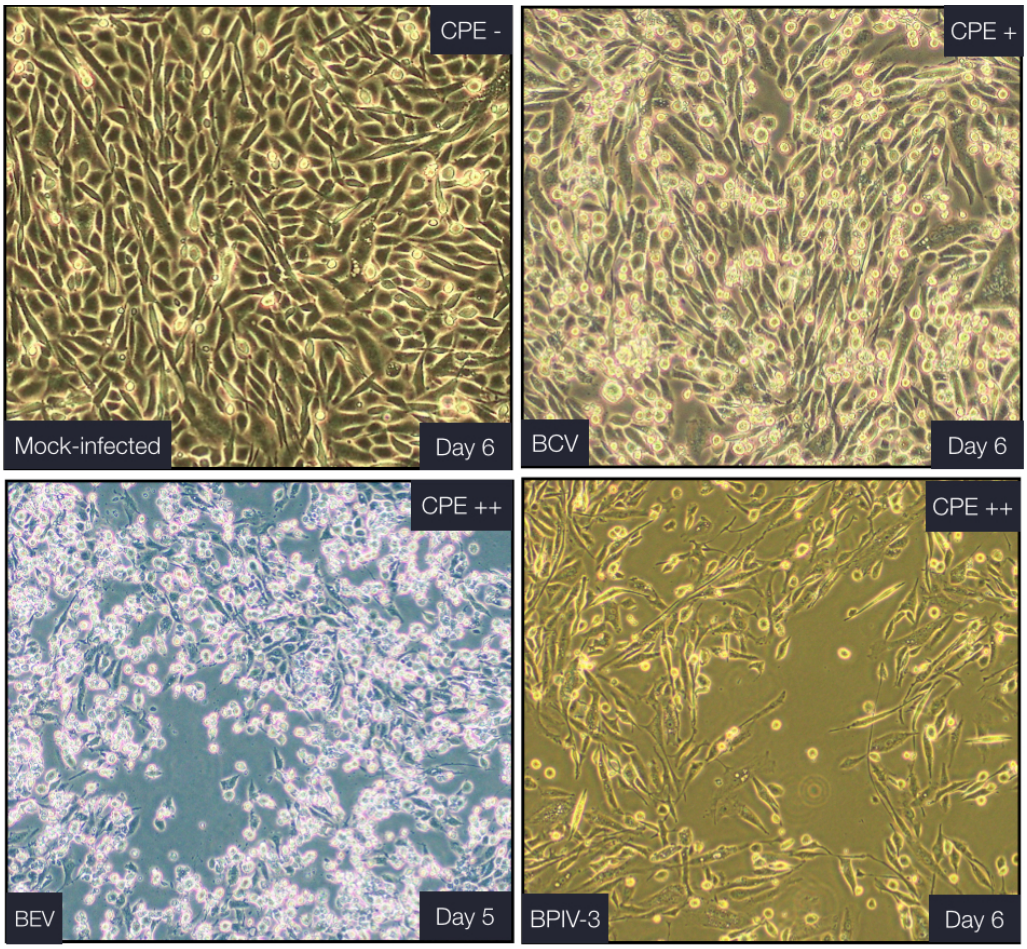
CPE -
Mock-infected
Day 6
CPE +
BCV
Day 6
CPE ++
BEV
Day 5
CPE ++
BPIV-3
Day 6

Continue…

Continued…

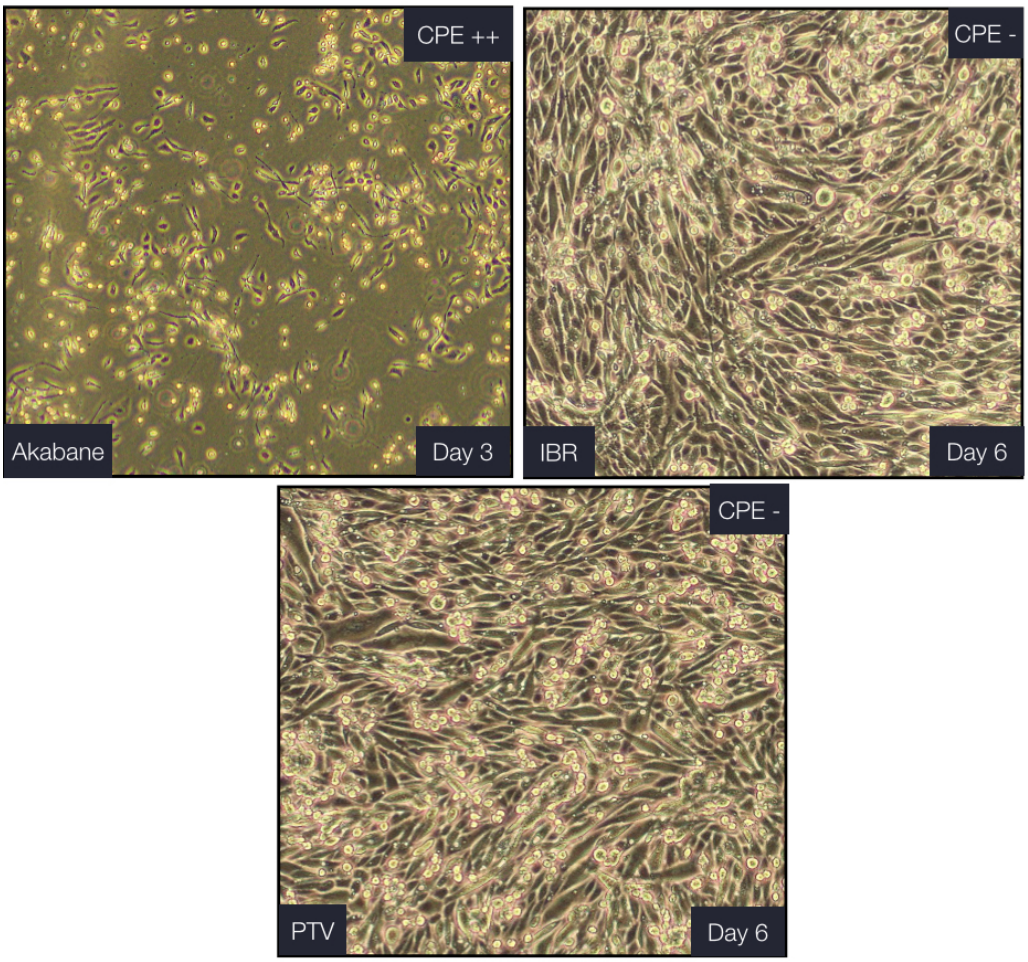


Fig. 2-5. The CPE morphology-based CPE appearance of BHK-ATeam infected cells. The bovine coronavirus (BCV) showed mild CPE at day 6 post-infection, bovine enterovirus (BEV) showed CPE at day 5 post-infection, bovine parainfluenza virus (BPIV3) showed CPE at day 6 post-infection, Akabane virus showed CPE at day 3 post-infection, while infectious bovine rhinotracheitis virus (IBR), and porcine teschovirus-ka2 (PTV-ka2) showed no CPE.

Table 2-1. The Venus/CFP (cyan fluorescent protein) ratio in Boomerang Catcher analyzed BHK-ATeam cells infected with selected virus for 3 hr.

| | Viruses | | | | | |
|---|---|---|---|---|---|---|
| MOI | AKV | BCV | BEV | BPIV3 | IBR | PTV |
| mock | 0.85 ± 0.02 | 0.80 ± 0.02 | 0.84 ± 0.03 | 0.76 ± 0.03 | 0.68 ± 0.03 | 0.83 ± 0.02 |
| 0.25 | 0.83 ± 0.01*** | 0.81 ± 0.03* | 0.85 ± 0.02* | 0.81 ± 0.02*** | 0.77 ± 0.03*** | 0.83 ± 0.02 |
| 0.75 | 0.85 ± 0.03 | 0.82 ± 0.02** | 0.85 ± 0.03** | 0.82 ± 0.03*** | 0.79 ± 0.03*** | 0.81 ± 0.02*** |
| 1.25 | 0.86 ± 0.03 | 0.83 ± 0.03 | 0.85 ± 0.03 | 0.82 ± 0.02*** | 0.80 ± 0.02*** | 0.81 ± 0.02*** |

More than 60 individual cells per each virus. Data; the mean ± S.D., Dunnet's test between virus infected cells versus the mock (* $p < 0.01$, ** $p < 0.001$, *** $p < 0.0001$). MOI: Multiplicity of infection, AKV: Akabane virus, BCV: bovine coronavirus, BEV: bovine enterovirus, BPIV3: bovine parainfluenza 3 virus, IBR: infectious bovine rhinotracheitis virus, PTV: porcine teschovirus,

Table 2-2. The qPCR result of viral-infected BHK-ATeam cells by selected viruses.

| Virus name | Incubation time | Cq |
|---|---|---|
| Bovine Coronavirus | 3h | 28.73 |
| | 6 days | 23.95 |
| | Negative Control | – |
| Bovine Enterovirus | 3h | 28.82 |
| | 6 days | 19.11 |
| | Negative Control | – |
| Infectious Bovine Rhinotracheitis Virus | 3h | 31.32 |
| | 6 days | 17.88 |
| | Negative Control | – |
| Bovine Parainfluenza virus-3 | 3h | 35.16 |
| | 6 days | 15.61 |
| | Negative Control | – |
| Porcine Teschovirus- ka2 | 3h | 28.03 |
| | 6 days | 26.77 |
| | Negative Control | 36.14 |
| Akabane virus | 3h | – |
| | 4 days | 20.66 |
| | Negative Control | – |

Cq: cycle number, –: negative

Table 2-3. The primers and probes used in this study

| **Virus name** | | **Primer/Probe sequence 5'-3' (FAM/TAMRA)** |
|---|---|---|
| Akabane virus | F | TCAACCAGAAGAAGGCCAAGAT |
| | R | GGGAAAATGGTTATTAACCACTGTAAA |
| | P | TTACATAAGACGCCACAACCA |
| Bovine coronavirus | F | CTGGAAGTTGGTGGAGTT |
| | R | ATTATCGGCCTAACATACATC |
| | P | CCTTCATATCTATACACATCAAGTTGTT |
| Bovine enterovirus | F | GCCGTGAATGCTGCTAATCC |
| | R | GTAGTCTGTTCCGCCTCCACCT |
| | P | CGCACAATCCAGTGTTGCTACGTCGTAAC |
| Bovine parainfluenza A virus | F | GCAATGCTGCAGGACTAGGTATAAT |
| | R | ACACTGTAATTGATGACCCCATTCT |
| | P | ACCAAGACTTGTATGATGCTGCCAAAGCA |
| Infectious bovine rhinotracheitis virus | F | CAATAACAGCGTAGACCTGGTC |
| | R | GCTGTAGTCCCAAGCTTCCAC |
| | P | TGCGGCCTCCGGGCTTTACGTCT |
| Porcine Teschovirus-ka2 | F | ACACAGAAGCCGCTCTTACT |
| | R | CAAAAGAGTTGCCAGCGGTC |

F: forward, R: reverse, P: probe

# General Discussion and Conclusion

In the presence of a stressful stimulus, the cellular initial response is directed towards coping with the insult by mounting an appropriate protective cellular response to ensure cell survival (Fulda et al., 2010). There are various pro-survival activities of the cell including the heat shock response, the unfolded protein response (UPR), the DNA damage response, and the response to oxidative stress all aimed at restoring the cellular homeostasis (Galluzzi et al., 2018; Hotamisligil and Davis, 2016; Fulda et al., 2010). Viruses, being an intracellular parasite, utilize cellular machinery and resources for their replication that consequently elicit cellular stress responses. It has been reported that various viruses such as African swine fever virus, cytomegalovirus, hepatitis B virus, papillomavirus, vaccinia virus, BVDV, JEV, and HCV modulate UPR by binding of the master control binding protein (BiP) to the accumulated misfolded or unfolded proteins leading to the release of endoplasmic reticulum (ER) transducers: PKR-like ER kinase (PERK), activating transcription factor 6 (ATF6), and the ER transmembrane protein kinase/endoribonuclease (IRE1) that subsequently leads to homodimerization and refolding of proteins (Jheng et al., 2014; He, 2006; Jordan et al., 2002). Furthermore, viruses cause ER stress by exploitation of the ER membrane (e.g., poliovirus, coxsackievirus B3, dengue virus and hepatitis C virus), accumulation of misfolded proteins (e.g., influenza A virus, hepatitis A virus, JEV, and HCV), imbalance of calcium concentration by viroporin (e.g., influenza A virus, coxsackievirus B3, poliovirus 1), and the sabotage or depletion of the ER membrane during virion release (e.g., rotavirus) (Jheng et al., 2014; Su et al., 2002). Viral infections also induce the formation of stress granules by cells, which are aggregates that contain preinitiation complexes where the translation is arrested, but interfered by

viruses like West Nile virus or dengue virus (Montero and Trujillo-Alonso, 2011). Viruses such as HCV, HIV, human adenovirus-5, Epstein-Barr virus, hepatitis B virus, and EMCV can induce reactive oxygen species (ROS) which directly or indirectly help them survive (Anand and Tikoo, 2013). All of these cellular responses affect the metabolites in the cell and require a lot of energy thus affecting the ATP level. In addition, many viruses can modulate mitochondrial-mediated pathways (Anand and Tikoo, 2013), which directly affects ATP. All of these protective cellular responses to viral infection requires ATP and thus, infected cells will also increase the generation of ATP to compensate for the loss until all resources are exhausted by the viruses leading to cell death. It is therefore logical to consider intracellular ATP level as an indication of viral invasion of cells and as an early sign of CPE.

In this study, all the viruses tested showed significantly different Venus/CFP ratio compared to mock as early as 3h although the pattern is not similar. In cases of BVDV, EMCV, JEV, PTV-ka2, and Akabane virus, the Venus/CFP ratio is significantly lower compared to mock. Conversely, the IBR, BCV, BEV, and BPIV3 showed significantly higher Venus/CFP ratio compared to mock. Thus, the intracellular ATP level is affected differently depending on the virus. This has been observed in other viruses wherein the infection by vaccinia virus (Chang et al., 2009), human cytomegalovirus (HCMV) (Munger et al., 2006), baculovirus (Olejnik et al., 2004) and avian reovirus (Chi et al., 2018) results in increased of ATP production; while infection hepatitis C virus (HCV) (Ando et al., 2012), influenza virus (Maruyama et al., 2018; Ritter et al., 2010), and dengue virus (El-Bacha et al., 2007), showed decrease of ATP due to active consumption. Regardless of the type of virus, the ATeam technology and subsequent analysis by BC showed ATP-based CPE in

viral-infected cells which appears more faster than the conventional morphology-based CPE.

In conclusion, ATeam technology is useful in determining the early sign of ATP-based CPE, as early as 3 h without visual CPE by light microscopy, and enables high throughput determination of the presence of microorganisms in neglected samples stored in laboratories. This novel method is useful for rapid viral isolation and detection in viral studies.

## ACKNOWLEDGEMENT

THE AUTHOR'S HEARTFELT GRATITUDE:

To Dr. Eiichi Hondo, her thesis supervisor, for the creative ideas, guidance, valuable suggestions and perseverance in checking her manuscript, and for helping her to be able to publish in high-tier journal.

To Dr. Tetsuya Mizutani, and Dr. Oba, the collaborators from Tokyo University of Agriculture and Technology, for preparing and submitting the samples and viruses for the improvement of her study.

To Dr. Hideki Shibata, for his valuable suggestions and for teaching the author on the basics on how to operate confocal microscopy as well as for guiding her in improving her confocal microscopic skills

To Dr. Tomoki Ishibashi, for his invaluable contribution to the development of the software program called Boomerang Catcher.

To Dr. Atsuo Iida, Dr. Hitoshi Takemae, Dr. Ken maeda, and Dr. Hiroshi Shimoda, for sharing their knowledge and constructive criticisms for the improvement of the manuscript.

To MEXT, for the financial support.

To her labmates for the assistance, emotional support, and for making the author's stay in Japan memorable.

To the Association of Filipino Student's in Nagoya, especially to Nona and Crusty, for the company, comfort, and advice during the author's down moments.

To Doysabas family, for the prayers, love, and inspiration.

To Lola Poling, for the unconditional love, care, and prayers.

To Mama Inday, for her undying support, unceasing care, and unfading love.

To God, the almighty Father, her omnipotent, omnipresent, and omniscient, whose providence in all forms never end.

Thank you very much!

**References**

Albas, A., Campos, A. C., Araujo, D. B., Rodrigues, C. S., Sodre, M. M., Durigon, E. L.,Favoretto, S. R., 2011. Molecular characterization of rabies virus isolated from non-haematophagous bats in Brazil. Rev Soc Bras Med Trop. 44**,** 678-683.

Albrecht, T., Fons, M., Boldogh, I.,Rabson, A. S. 1996. Effects on cells. In *Medical microbiology,* ed. S. Baron. Galveston, Texas, USA: Univ of Texas Medical Branch.

Almeida, M. F., Favoretto, S. R., Martorelli, L. F., Trezza-Netto, J., Campos, A. C., Ozahata, C. H., Sodre, M. M., Kataoka, A. P., Sacramento, D. R.,Durigon, E. L., 2011. Characterization of rabies virus isolated from a colony of *Eptesicus furinalis* bats in Brazil. Rev Inst Med Trop Sao Paulo. 53**,** 31-37.

Almeida, M. F., Martorelli, L. F. A., Aires, C. C., Sallum, P. C., Durigon, E. L.,Massad, E., 2005. Experimental rabies infection in haematophagous bats *Desmodus rotundus*. Epidemiology and Infection. 133**,** 523-527. 10.1017/s0950268804003656

Anand, S. K.,Tikoo, S. K., 2013. Viruses as modulators of mitochondrial functions. Advances in Virology. 2013**,** 738794. 10.1155/2013/738794

Ando, T., Imamura, H., Suzuki, R., Aizaki, H., Watanabe, T., Wakita, T.,Suzuki, T., 2012. Visualization and measurement of ATP levels in living cells replicating hepatitis C virus genome RNA. PLoS Pathog. 8**,** e1002561. 10.1371/journal.ppat.1002561

Anindita, P. D., Sasaki, M., Setiyono, A., Handharyani, E., Orba, Y., Kobayashi, S., Rahmadani, I., Taha, S., Adiani, S., Subangkit, M., Nakamura, I., Sawa,

H.,Kimura, T., 2015. Detection of coronavirus genomes in moluccan naked-backed fruit bats in Indonesia. Arch Virol. 160**,** 1113-8. 10.1007/s00705-015-2342-1

Annan, A., Baldwin, H. J., Corman, V. M., Klose, S. M., Owusu, M., Nkrumah, E. E., Badu, E. K., Anti, P., Agbenyega, O., Meyer, B., Oppong, S., Sarkodie, Y. A., Kalko, E. K., Lina, P. H., Godlevska, E. V., Reusken, C., Seebens, A., Gloza-Rausch, F., Vallo, P., Tschapka, M., Drosten, C., Drexler, J. F., 2013. Human betacoronavirus 2c EMC/2012-related viruses in bats, Ghana and Europe. Emerg Infect Dis. 19**,** 456-459. 10.3201/eid1903.121503

Anthony, S. J., Gilardi, K., Menachery, V. D., Goldstein, T., Ssebide, B., Mbabazi, R., Navarrete-Macias, I., Liang, E., Wells, H., Hicks, A., Petrosov, A., Byarugaba, D. K., Debbink, K., Dinnon, K. H., Scobey, T., Randell, S. H., Yount, B. L., Cranfield, M., Johnson, C. K., Baric, R. S., Lipkin, W. I., Mazet, J. A., 2017. Further evidence for bats as the evolutionary source of Middle East respiratory syndrome coronavirus. MBio. 8. 10.1128/mBio.00373-17

Anthony, S. J., Ojeda-Flores, R., Rico-Chavez, O., Navarrete-Macias, I., Zambrana-Torrelio, C. M., Rostal, M. K., Epstein, J. H., Tipps, T., Liang, E., Sanchez-Leon, M., Sotomayor-Bonilla, J., Aguirre, A. A., Avila-Flores, R., Medellin, R. A., Goldstein, T., Suzan, G., Daszak, P., Lipkin, W. I., 2013. Coronaviruses in bats from Mexico. J Gen Virol. 94**,** 1028-1038. 10.1099/vir.0.049759-0

Bashir, S., Dar, A. M., Bhat, A. A., Bukhari, S., Hussain, T., Yadav, K. S., Ahmed, A., 2015. Isolation of infectious bovine rhinotracheitis virus in cell culture: (a case study). Journal of Cell and Tissue Research. 15**,** 5063-5066.

Breed, A. C., Breed, M. F., Meers, J., Field, H. E., 2011. Evidence of endemic hendra virus infection in flying-foxes (*Pteropus conspicillatus*)--implications for

disease risk management. PLoS One. 6**,** e28816. 10.1371/journal.pone.0028816

Burgener, A., Coombs, K.,Butler, M., 2006. Intracellular ATP and total adenylate concentrations are critical predictors of reovirus productivity from Vero cells. Biotechnol Bioeng. 94**,** 667-679. 10.1002/bit.20873

Chang, C. W., Li, H. C., Hsu, C. F., Chang, C. Y.,Lo, S. Y., 2009. Increased ATP generation in the host cell is required for efficient vaccinia virus production. J Biomed Sci. 16**,** 80. 10.1186/1423-0127-16-80

Chen, Y. N., Phuong, V. N., Chen, H. C., Chou, C. H., Cheng, H. C., Wu, C. H., 2016. Detection of the severe acute respiratory syndrome-related coronavirus and alphacoronavirus in the bat population of Taiwan. Zoonoses Public Health. 63**,** 608-615. 10.1111/zph.12271

Chi, P. I., Huang, W. R., Chiu, H. C., Li, J. Y., Nielsen, B. L., Liu, H. J., 2018. Avian reovirus σA-modulated suppression of lactate dehydrogenase and upregulation of glutaminolysis and the mTOC1/eIF4E/HIF-1α pathway to enhance glycolysis and the TCA cycle for virus replication. Cell Microbiol. 20**,** e12946. 10.1111/cmi.12946

Chuang, C., Prasanth, K. R., Nagy, P. D., 2017. The glycolytic pyruvate kinase is recruited directly into the viral replicase complex to generate ATP for RNA synthesis. Cell Host & Microbe. 22**,** 639-652. 10.1016/j.chom.2017.10.004

Conley, J. M., Radhakrishnan, S., Valentino, S. A., Tantama, M., 2017. Imaging extracellular ATP with a genetically-encoded, ratiometric fluorescent sensor. PLoS One. 12**,** e0187481. 10.1371/journal.pone.0187481

Davis, A. D., Gordy, P. A., Bowen, R. A., 2013a. Unique characteristics of bat rabies viruses in big brown bats (eptesicus fuscus). Arch Virol. 158**,** 809-820. 10.1007/s00705-012-1551-0

Davis, A. D., Jarvis, J. A., Pouliott, C., Rudd, R. J., 2013b. Rabies virus infection in *Eptesicus fuscus* bats born in captivity (naive bats). PLoS One. 8**,** e64808. 10.1371/journal.pone.0064808

Depaoli, M. R., Karsten, F., Madreiter-Sokolowski, C. T., Klec, C., Gottschalk, B., Bischof, H., Eroglu, E., Waldeck-Weiermair, M., Simmen, T., Graier, W. F., Malli, R., 2018. Real-time imaging of mitochondrial ATP dynamics reveals the metabolic setting of single cells. Cell Reports. 25**,** 502-512. 10.1016/j.celrep.2018.09.027

Diamond, D. L., Syder, A. J., Jacobs, J. M., Sorensen, C. M., Walters, K. A., Proll, S. C., McDermott, J. E., Gritsenko, M. A., Zhang, Q., Zhao, R., Metz, T. O., Camp, D. G., 2nd, Waters, K. M., Smith, R. D., Rice, C. M., Katze, M. G., 2010. Temporal proteome and lipidome profiles reveal hepatitis C virus-associated reprogramming of hepatocellular metabolism and bioenergetics. PLoS Pathog. 6**,** e1000719. 10.1371/journal.ppat.1000719

El-Bacha, T., Midlej, V., Pereira da Silva, A. P., Silva da Costa, L., Benchimol, M., Galina, A., Da Poian, A. T., 2007. Mitochondrial and bioenergetic dysfunction in human hepatic cells infected with dengue 2 virus. Biochim Biophys Acta. 1772**,** 1158-1166. 10.1016/j.bbadis.2007.08.003

Enders, J. F., Weller, T. H., Robbins, F. C., 1949. Cultivation of the lansing strain of poliomyelitis virus in cultures of various human embryonic tissues. Science. 109**,** 85-87. 10.1126/science.109.2822.85

Enquist, L. W., Racaniello, V. R. 2013. Virology: From contagium fluidum to virome. In *Fields virology,* eds. D. M. Knipe & P. M. Howley. PA, USA: Lippincott Williams & Wilkins.

Findlay, J. S., Ulaeto, D., 2015. Semliki Forest virus and Sindbis virus, but not vaccinia virus, require glycolysis for optimal replication. J Gen Virol. 96**,** 2693-2696. 10.1099/jgv.0.000226

Fontaine, K. A., Sanchez, E. L., Camarda, R., Lagunoff, M., 2015. Dengue virus induces and requires glycolysis for optimal replication. J Virol. 89**,** 2358-66. 10.1128/JVI.02309-14

Fulda, S., Gorman, A. M., Hori, O., Samali, A., 2010. Cellular stress responses: Cell survival and cell death. Int J Cell Biol. 2010**,** 214074. 10.1155/2010/214074

Galluzzi, L., Yamazaki, T., Kroemer, G., 2018. Linking cellular stress responses to systemic homeostasis. Nat Rev Mol Cell Biol. 19**,** 731-745. 10.1038/s41580-018-0068-0

Goodwin, C. M., Xu, S., Munger, J., 2015. Stealing the keys to the kitchen: Viral manipulation of the host cell metabolic network. Trends Microbiol. 23**,** 789-798. 10.1016/j.tim.2015.08.007

Gurer, C., Hoglund, A., Hoglund, S., Luban, J., 2005. ATPγS disrupts human immunodeficiency virus type 1 virion core integrity. J Virol. 79**,** 5557-5567. 10.1128/JVI.79.9.5557-5567.2005

He, B., 2006. Viruses, endoplasmic reticulum stress, and interferon responses. Cell Death Differ. 13**,** 393-403. 10.1038/sj.cdd.4401833

Hematian, A., Sadeghifard, N., Mohebi, R., Taherikalani, M., Nasrolahi, A., Amraei, M., Ghafourian, S., 2016. Traditional and modern cell culture in virus diagnosis. Osong Public Health Res Perspect. 7**,** 77-82. 10.1016/j.phrp.2015.11.011

Hotamisligil, G. S., Davis, R. J., 2016. Cell signaling and stress responses. Cold Spring Harb Perspect Biol. 8. 10.1101/cshperspect.a006072

Hui, E. K., Nayak, D. P., 2001. Role of ATP in influenza virus budding. Virology. 290**,** 329-341. 10.1006/viro.2001.1181

Imamura, H., Huynh Nhat, K. P., Togawa, H., Saito, K., Iino, R., Kato-Yamada, Y., Nagai, T., Noji, H., 2009. Visualization of ATP levels inside single living cells with fluorescence resonance energy transfer-based genetically encoded indicators. PNAS. 106**,** 15651–15656. 10.1073/pnas.0904764106

Itakura, Y., Matsuno, K., Ito, A., Gerber, M., Liniger, M., Fujimoto, Y., Tamura, T., Kameyama, K. I., Okamatsu, M., Ruggli, N., Kida, H., Sakoda, Y., 2019. A cloned classical swine fever virus derived from the vaccine strain GPE- causes cytopathic effect in CPK-NS cells via type-I interferon-dependent necroptosis. Virus Res. 276**,** 197809. 10.1016/j.virusres.2019.197809

Jheng, J. R., Ho, J. Y., Horng, J. T., 2014. ER stress, autophagy, and RNA viruses. Front Microbiol. 5**,** 388. 10.3389/fmicb.2014.00388

Jordan, R., Wang, L., Graczyk, T. M., Block, T. M.,Romano, P. R., 2002. Replication of a cytopathic strain of bovine viral diarrhea virus activates PERK and induces endoplasmic reticulum stress-mediated apoptosis of MDBK cells. J Virol. 76**,** 9588-9599. 10.1128/jvi.76.19.9588-9599.2002

Khushbu,Vats, I., 2017. Otsu image segmentation algorithm: A review. International Journal of Innovative Research in Computer and Communication Engineering. 5**,** 11945-11948 10.15680/IJIRCCE.2017

Kishimoto, M., Tsuchiaka, S., Rahpaya, S. S., Hasebe, A., Otsu, K., Sugimura, S., Kobayashi, S., Komatsu, N., Nagai, M., Omatsu, T., Naoi, Y., Sano, K., Okazaki-Terashima, S., Oba, M., Katayama, Y., Sato, R., Asai, T., Mizutani, T., 2017. Development of a one-run real-time PCR detection system for pathogens associated with bovine respiratory disease complex. J. Vet. Med. Sci. 79**,** 512-523. 10.1292/jvms.16-0489

Klumpp, K., Ford, M. J., Ruigrok, R. W., 1998. Variation in ATP requirement during influenza virus transcription. Journal of General Virology. 79**,** 1033-1045. 10.1099/0022-1317-79-5-1033

Kowalski, M., Bergeron, L., Dorfman, T., Haseltine, W.,Sodroski, J., 1991. Attenuation of human immunodeficiency virus type 1 cytopathic effect by a mutation affecting the transmembrane envelope glycoprotein. Journal of Virology. 65**,** 281-291.

Lau, S. K., Woo, P. C., Lai, K. K., Huang, Y., Yip, C. C., Shek, C. T., Lee, P., Lam, C. S., Chan, K. H., Yuen, K. Y., 2011. Complete genome analysis of three novel picornaviruses from diverse bat species. J Virol. 85**,** 8819-8828. 10.1128/JVI.02364-10

Leland, D. S., Ginocchio, C. C., 2007. Role of cell culture for virus detection in the age of technology. Clin Microbiol Rev. 20**,** 49-78. 10.1128/CMR.00002-06

Lerchundi, R., Kafitz, K. W., Winkler, U., Farfers, M., Hirrlinger, J., Rose, C. R., 2018. FRET-based imaging of intracellular atp in organotypic brain slices. J Neurosci Res. 10.1002/jnr.24361

Leroy, E. M., Epelboin, A., Mondonge, V., Pourrut, X., Gonzalez, J. P., Muyembe-Tamfum, J. J., Formenty, P., 2009. Human ebola outbreak resulting from direct exposure to fruit bats in Luebo, Democratic Republic of Congo, 2007. Vector Borne Zoonotic Dis. 9**,** 723-8. 10.1089/vbz.2008.0167

Leroy, E. M., Kumulungui, B., Pourrut, X., Rouquet, P., Hassanin, A., Yaba, P., Delicat, A., Paweska, J. T., Gonzalez, J. P., Swanepoel, R., 2005. Fruit bats as reservoirs of ebola virus. Nature. 438**,** 575-576. 10.1038/438575a

Li, P. P., Itoh, N., Watanabe, M., Shi, Y., Liu, P., Yang, H. J.,Kasamatsu, H., 2008. Association of simian virus 40 vp1 with 70-kilodalton heat shock proteins and viral tumor antigens. Journal of Virology. 83**,** 37-46. 10.1128/jvi.00844-08

MacLachlan, N. J.,Dubovi, E. J. 2011. *Fenner's veterinary virology* CA, USA: Academic press.

Mahmoudabadi, G., Milo, R., Phillips, R., 2017. Energetic cost of building a virus. Proc Natl Acad Sci U S A. 114**,** E4324-E4333. 10.1073/pnas.1701670114

Maitland, H. B., 1928. Cultivation of vaccinia virus without tissue culture. Lancet. 2**,** 596-597.

Maruyama, H., Kimura, T., Liu, H., Ohtsuki, S., Miyake, Y., Isogai, M., Arai, F., Honda, A., 2018. Influenza virus replication raises the temperature of cells. Virus Res. 257**,** 94-101. 10.1016/j.virusres.2018.09.011

Montero, H., Trujillo-Alonso, V., 2011. Stress granules in the viral replication cycle. Viruses. 3**,** 2328-2338. 10.3390/v3112328

Morita, S., Kojima, T., Kitamura, T., 2000. Plat-E: An efficient and stable system for transient packaging of retroviruses. Gene Ther. 7**,** 1063-1066. 10.1038/sj.gt.3301206

Munger, J., Bajad, S. U., Coller, H. A., Shenk, T., Rabinowitz, J. D., 2006. Dynamics of the cellular metabolome during human cytomegalovirus infection. PLoS Pathog. 2**,** e132. 10.1371/journal.ppat.0020132

Nakano, M., Imamura, H., Nagai, T., Noji, H., 2011. Ca(2)(+) regulation of mitochondrial ATP synthesis visualized at the single cell level. ACS Chem Biol. 6**,** 709-15. 10.1021/cb100313n

Nomaguchi, M., Ackermann, M., Yon, C., You, S., Padmanabhan, R., 2003. De novo synthesis of negative-strand RNA by dengue virus RNA-dependent RNA polymerase in vitro: Nucleotide, primer, and template parameters. J Virol. 77**,** 8831-42. 10.1128/jvi.77.16.8831-8842.2003

Oba, M., Naoi, Y., Ito, M., Masuda, T., Katayama, Y., Sakaguchi, S., Omatsu, T., Furuya, T., Yamasato, H., Sunaga, F., Makino, S., Mizutani, T., Nagai, M., 2018. Metagenomic identification and sequence analysis of a teschovirus A-related virus in porcine feces in japan, 2014-2016. Infect Genet Evol. 66**,** 210-216. 10.1016/j.meegid.2018.10.004

Olejnik, A. M., Czaczyk, K., Marecik, R., Grajek, W., Jankowski, T., 2004. Monitoring the progress of infection and recombinant protein production in insect cell cultures using intracellular ATP measurement. Appl Microbiol Biotechnol. 65**,** 18-24. 10.1007/s00253-003-1550-x

Papafragkou, E., Hewitt, J., Park, G. W., Greening, G., Vinje, J., 2014. Challenges of culturing human norovirus in three-dimensional organoid intestinal cell culture models. PLoS One. 8**,** e63485. 10.1371/journal.pone.0063485

Rahman, S. A., Hassan, S. S., Olival, K. J., Mohamed, M., Chang, L. Y., Hassan, L., Saad, N. M., Shohaimi, S. A., Mamat, Z. C., Naim, M. S., Epstein, J. H., Suri, A. S., Field, H. E., Daszak, P., Henipavirus Ecology Research, G., 2010. Characterization of nipah virus from naturally infected *Pteropus vampyrus* bats, malaysia. Emerg Infect Dis. 16**,** 1990-1993. 10.3201/eid1612.091790

Rahpaya, S. S., Tsuchiaka, S., Kishimoto, M., Oba, M., Katayama, Y., Nunomura, Y., Kokawa, S., Kimura, T., Kobayashi, A., Kirino, Y., Okabayashi, T., Nonaka, N., Mekata, H., Aoki, H., Shiokawa, M., Umetsu, M., Morita, T., Hasebe, A., Otsu, K., Asai, T., Yamaguchi, T., Makino, S., Murata, Y., Abi, A. J., Omatsu, T.,Mizutani, T., 2018. Dembo polymerase chain reaction technique for detection of bovine abortion, diarrhea, and respiratory disease complex infectious agents in potential vectors and reservoirs. J Vet Sci. 19**,** 350-357. 10.4142/jvs.2018.19.3.350

Rajput, M. K. S., Abdelsalam, K., Darweesh, M. F., Braun, L. J., Kerkvliet, J., Hoppe, A. D., Chase, C. C. L., 2017. Both cytopathic and non-cytopathic bovine viral diarrhea virus (bvdv) induced autophagy at a similar rate. Vet Immunol Immunopathol. 193-194**,** 1-9. 10.1016/j.vetimm.2017.09.006

Ritter, J. B., Wahl, A. S., Freund, S., Genzel, Y., Reichl, U., 2010. Metabolic effects of influenza virus infection in cultured animal cells: intra- and extracellular metabolite profiling. BMC Systems Biology. 4**,** 1-22. 10.1186/1752-0509-4-6

Robbins, F. J., Enders, J. F., Weller, T. H., 1950. Cytopathogenic effect of poliomyelitis viruses in vitro on human embryonic tissues. Prceedings of the Society for Experimental Biology and Medicine. 75**,** 370-374. 10.3181/00379727-75-18202

Roche, S. E., Costard, S., Meers, J., Field, H. E., Breed, A. C., 2015. Assessing the risk of nipah virus establishment in Australian flying-foxes. Epidemiol Infect. 143**,** 2213-26. 10.1017/S0950268813003336

Su, H. L., Liao, C. L., Lin, Y. L., 2002. Japanese encephalitis virus infection initiates endoplasmic reticulum stress and an unfolded protein response. J Virol. 76**,** 4162-4171. 10.1128/jvi.76.9.4162-4171.2002

Toloe, J., Mollajew, R., Kugler, S., Mironov, S. L., 2014. Metabolic differences in hippocampal 'Rett' neurons revealed by ATP imaging. Mol Cell Neurosci. 59**,** 47-56. 10.1016/j.mcn.2013.12.008

Tsuchiaka, S., Masuda, T., Sugimura, S., Kobayashi, S., Komatsu, N., Nagai, M., Omatsu, T., Furuya, T., Oba, M., Katayama, Y., Kanda, S., Yokoyama, T., Mizutani, T., 2015. Development of a novel detection system for microbes from bovine diarrhea by real-time PCR. J. Vet. Med. Sci. 78**,** 383-389. 10.1292/jvms.15-0552

Tsuyama, T., Kishikawa, J., Han, Y. W., Harada, Y., Tsubouchi, A., Noji, H., Kakizuka, A., Yokoyama, K., Uemura, T., Imamura, H., 2013. In vivo fluorescent adenosine 5'-triphosphate (ATP) imaging of *Drosophila melanogaster* and *Caenorhabditis elegans* by using a genetically encoded fluorescent ATP biosensor optimized for low temperatures. Anal Chem. 85**,** 7889-7896. 10.1021/ac4015325

Vreede, F. T., Gifford, H., Brownlee, G. G., 2008. Role of initiating nucleoside triphosphate concentrations in the regulation of influenza virus replication and transcription. Journal of Virology. 82**,** 6902-6910. 10.1128/jvi.00627-08

Woodruff, A. M., Goodpasture, E. W., 1931. The susceptibility of the chorio-allantoic membrane of chick embryos to infection with the fowl-pox virus. Am J Pathol. 7**,** 209-222.5.

Wu, Z., Ren, X., Yang, L., Hu, Y., Yang, J., He, G., Zhang, J., Dong, J., Sun, L., Du, J., Liu, L., Xue, Y., Wang, J., Yang, F., Zhang, S., Jin, Q., 2012. Virome analysis for identification of novel mammalian viruses in bat species from chinese provinces. J Virol. 86**,** 10999-1012. 10.1128/JVI.01394-12